

Communication-Aware Orbit Design for Small Spacecraft Swarms around Small Bodies

Federico Rossi* and Saptarshi Bandyopadhyay†

Jet Propulsion Laboratory, California Institute of Technology, 4800 Oak Grove Drive, Pasadena, CA 91109, USA

Mark Mote‡

Georgia Institute of Technology, 301 Ferst St., Atlanta, GA 30332, USA.

Jean-Pierre de la Croix§ and Amir Rahmani¶

Jet Propulsion Laboratory, California Institute of Technology, 4800 Oak Grove Drive, Pasadena, CA 91109, USA

Exploration of small Solar System bodies has traditionally been performed by monolithic spacecraft carrying several science instruments. However, instruments often cannot be operated simultaneously due to requirements including viewing angle, illumination, power, and data constraints. This has motivated interest in architectures where a swarm of small spacecraft, each carrying one instrument, studies a small body after being deployed by a carrier spacecraft; such architectures hold promise to yield significant improvements in mission efficiency, increased data quality, and reduced mission duration. A key difficulty is the selection of orbits for the spacecraft, which must satisfy not only instrument requirements, but also communication and data storage constraints. To address this, we propose a novel gradient-based optimization algorithm that simultaneously optimizes spacecraft orbits, observations, and communications; the approach captures instrument requirements, communication bandwidth, and memory usage, and accommodates irregular gravity field models and surface geometries. Numerical simulations of a six-spacecraft swarm studying 433 Eros show that the approach results in a 67.9% increase in data returned compared to a communication-agnostic approach. Collectively, these results enable system designers to quickly assess the end-to-end performance of multi-spacecraft constellations, and represent a first step toward communication-aware design of multi-spacecraft missions for small Solar System body exploration.

A preliminary version of this paper was presented at the 2020 AIAA/AAS Astrodynamics Specialist Conference, August 9-12, 2020, held virtually, as paper AAS 20-603 [1].

*Robotics Technologist, Maritime and Multi-Agent Autonomy Group. M/S 198-219. AIAA Member

†Robotics Technologist, Maritime and Multi-Agent Autonomy Group. M/S 198-219.

‡Graduate Research Assistant, Department of Aerospace Engineering

§Robotics Systems Engineer, Maritime and Multi-Agent Autonomy Group. M/S 198-219. AIAA Member

¶Robotics Systems Engineer, Maritime and Multi-Agent Autonomy Group. M/S 198-219. AIAA Senior Member

I. Introduction

In recent years, a number of missions have explored small Solar System bodies such as asteroids and comets (e.g. Rosetta [2], Hayabusa 1&2 [3, 4], and Osiris-Rex [5]). The spacecraft performing these missions carry a number of science instruments to study the small body; however, only a small number of instruments can typically be operated simultaneously, due to constraints including viewing angle and sun angle requirements, range and ground resolution considerations, and power and storage constraints. Moreover, the orbital parameters best suited to collect data vary widely among instruments, resulting in complex operations, the need to execute costly orbital maneuvers, and inevitable sacrifices in the quality of the data collected by some instruments.

Swarms of small spacecraft, where each spacecraft carries a single science instrument, hold promise to perform science missions in this class more efficiently compared to monolithic architectures, resulting in better data quality, shorter mission duration, and additional robustness to failures of individual vehicles.

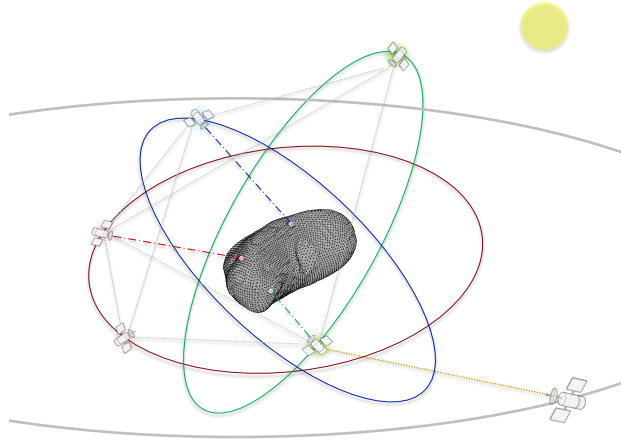


Fig. 1 A notional mission with 6 spacecraft orbiting around 433 Eros. The spacecraft conduct observations of the asteroid and communicate the data to the carrier, which relays it to Earth.

One such mission concept is shown in Fig. 1. A carrier spacecraft, which is responsible for deploying the instrument-carrying spacecraft and relaying data from the entire swarm back to Earth, orbits near the small body. Multiple small spacecraft are deployed by the carrier in selected orbits around the small body; each spacecraft carries one science instrument, a radio allowing it to communicate with other spacecraft and with the carrier, and limited on-board memory. To collect data, each instrument-carrying spacecraft's orbit must satisfy the science instrument's viewing-angle, sun-angle, and altitude constraints (shown in Table 1 for a notional reference mission). As the spacecraft collect data, they relay it to the carrier, possibly through multiple communication hops. We assume that individual small spacecraft are unable to communicate directly with Earth, due to low-power radios and small-size antennas; therefore, all data collected by the spacecraft must be relayed to the carrier in order to be transmitted to Earth.

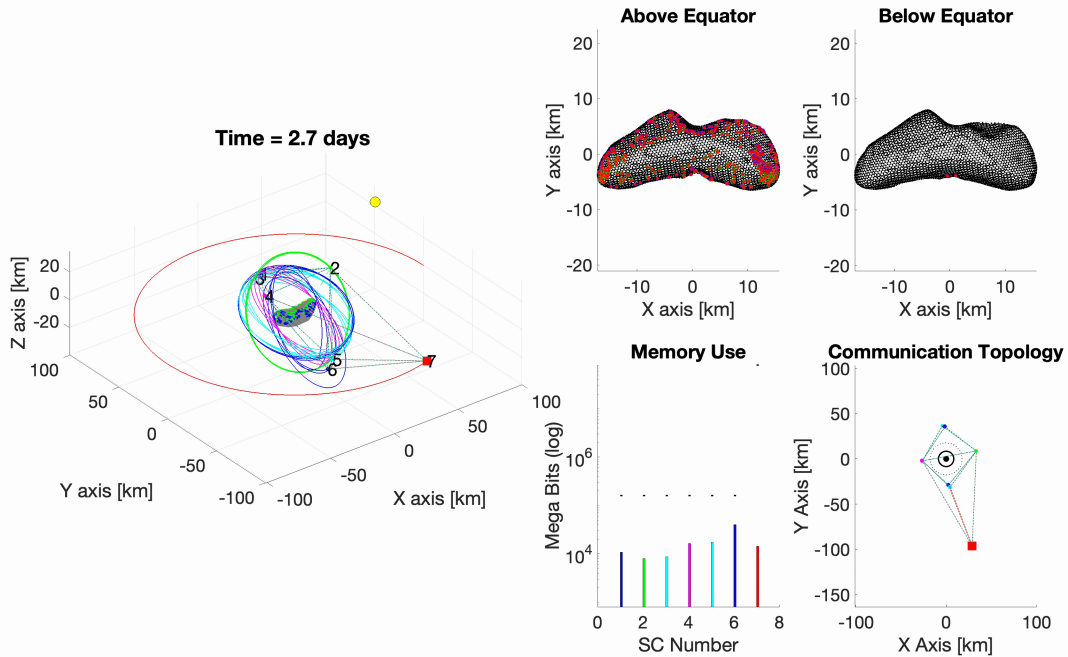


Fig. 2 Output of the optimization framework. The approach simultaneously optimizes observations, inter-spacecraft communication flows, and spacecraft orbits, maximizing the amount of scientific data relayed to the carrier spacecraft.

To realize this vision, it is necessary to devise orbit design algorithms that can optimize the orbits of each instrument-carrying spacecraft, accounting not only for the individual instruments’ requirements but also for communication constraints, i.e., the ability to return data to a carrier spacecraft in a timely manner, which is affected by inter-spacecraft bandwidths. Furthermore, it is desirable for these algorithms to be computationally efficient, so as to enable ground operators to redesign orbits as more information is gathered about the small body’s gravitational dynamics. The goal of this paper is to address this challenge by developing an efficient optimization framework for *communication-aware multi-spacecraft orbit design* tailored to small body dynamics.

A. State of the Art

The problem of orbit design for constellations of spacecraft has seen a significant amount of interest in the scientific community, and a number of techniques for constellation design *in Earth orbit* exist. We refer the reader to [11–13] for excellent overviews with historical perspective. However, constellation design techniques for Earth orbit tend to heavily exploit the regular form of the planet’s gravity field; in contrast, the gravity field in close proximity of small bodies is highly irregular, making analytical and semi-analytical approaches infeasible. Small spacecraft constellation design using invariant manifolds has been proposed for lunar radio interferometer missions [14]. Numerical approaches are also used for orbit design for specific missions: for instance, particle swarm optimization is used to design the orbits of

Instrument	High Level Science Context	Measurement	Sun Angle [deg]	View Angle [deg]	Distance [km]	Surface Resolution	Data per pixel [bits]	Pixels per region	Data per region	Total Data
Imaging Spectrometer	Origin and formation of the solar system	Elemental composition of body	$-45^\circ, 0^\circ, 45^\circ$	$[-5^\circ, 5^\circ]$	[0, 50]	1m	360×16 (0.4 – 4 μ m range, 10nm resolution)	$1.103e5$	79.4 MB	0.81 TB
X-Ray Spectrometer	Origin and formation of the solar system	Elemental composition of body	$-45^\circ, 0^\circ, 45^\circ$	$[-5^\circ, 5^\circ]$	[0, 50]	10m (1')	60×16 (0.75–6.5keV range, 100eV resolution)	$1.103e3$	0.13 MB	1.34 GB
Camera	Chronology of the solar system, secondary processes	Photogeology (texture, color, size, shape)	$-45^\circ, 0^\circ, 45^\circ$	$[-10^\circ, 10^\circ]$	[0, 50]	10cm	3×16	$1.103e7$	66.2 MB	0.67 TB
Altimeter	Dynamics of small bodies	Topography	Any	$[-5^\circ, 5^\circ]$	[0, 50]	10cm	1×16	$1.103e7$	22.1 MB	0.22 TB

Table 1 Science traceability matrix and surface science instruments for a notional mission to 433 Eros. Each spacecraft carries a single science instrument. The STM and instruments are based on the NEAR Shoemaker [6] and Dawn [7] missions, and in line with recent work on multi-spacecraft exploration of small bodies [8–10].

six smallsats for the Sun Radio Interferometer Space Experiment (SunRISE) mission in a GEO graveyard orbit [15]. Design of orbits around small bodies has seen significant interest in recent years, with works focusing on designing swarms of small spacecraft to estimate the gravity field around asteroid with very high accuracy [9, 10, 16], deploy the spacecraft in passive collision-free orbits [17, 18], and conduct bistatic radar measurements for tomography [19]. However, such approaches do not explicitly account for *communication* between the spacecraft, which introduces a critical coupling between the individual vehicles’ orbits. In contrast, the approach proposed in this paper (i) allows for simultaneous optimization of *multiple* spacecraft’s orbits, explicitly accounting for the coupling introduced by communications, and (ii) can accommodate arbitrary irregular gravity fields (so long as a state-transition matrix can be computed numerically).

B. Contribution

Our contribution is threefold. First, we propose an efficient communication-aware observation optimization framework that simultaneously optimizes the observations captured by the spacecraft and the inter-spacecraft data flows for a *given* set of orbits, maximizing the amount of scientific data relayed to the carrier spacecraft (and, in turn, to Earth). The optimization approach models Delay Tolerant Networking-like [20] inter-spacecraft communication with limited on-board memory, and it captures instrument coverage, illumination, and geometry constraints. We also propose a linear relaxation of the problem, and show through numerical simulations that the relaxation yields high-quality solutions close to the optimum and can be solved in minutes on a commodity workstation.

Second, we turn our attention to the problem of orbit design. We leverage the differentiable nature of the linear relaxation of the observation optimizer, and the numerically-computed state transition matrix (efficiently computed through JPL’s Small-Body Dynamics Toolkit [21]), to compute the *gradient* of the solution with respect to the spacecraft’s

initial conditions with minimal computational overhead. We then use a gradient-based global search algorithm to identify high-quality orbits for the swarm that approximately maximize the amount of scientific data returned to the carrier, while remaining collision-free over the optimization period of interest (ensuring that the orbits remain collision-free *beyond* the optimization horizon is a critical direction for future research, and is discussed in Section V).

Third, we assess the performance of our optimization framework on a representative scenario of a multi-spacecraft, multi-instrument mission to 433 Eros (shown in Figure 2); we show that the proposed approach can increase scientific returns by almost 70% compared to a baseline communication-agnostic optimization approach.

Collectively, these results enable system designers to quickly assess the end-to-end performance of multi-spacecraft constellations, and represent a first step toward communication-aware design of multi-spacecraft missions for exploration of small Solar System bodies.

An implementation of our algorithm is available under a permissive open-source license at <https://github.com/nasa/icc>.

C. Organization

The rest of this paper is organized as follows. In Section II, we rigorously state the problem of communication-aware multi-spacecraft orbit design. In Section III, we outline a mixed-integer linear programming formulation that can be employed to solve the simpler problem of communication-aware observation scheduling for *fixed* orbits, and propose a linear relaxation of the problem; the sensitivity of the relaxation to the initial conditions is assessed analytically in Section IV. In Section V, we propose a multi-start gradient-based global optimization approach to solve the communication-aware multi-spacecraft orbit design problem; the approach uses the linear relaxation and, crucially, its sensitivity, to guide the optimization process. Numerical results in Section VI show that the proposed approach can significantly outperform communication-agnostic techniques in communication-constrained settings, and that the computational complexity of the approach is modest. Finally, in Section VII, we present our conclusions and propose directions for future research.

II. Problem Statement

Current small-body exploration missions all build around one monolithic spacecraft, with multiple instruments gathering the scientific data over multiple mission phases and relaying this data back to Earth through the Deep Space Network when communication opportunities arise. In contrast, multiple small spacecraft concurrently collecting the scientific data not only have to coordinate their motion to maximize the amount of data collected, but also have to consider inter-spacecraft communication bandwidth and available on-board memory to be able to relay the collected data to the carrier spacecraft, the designated Deep Space network Communicator with Earth. Hence, it is desirable to optimize for the largest joint coverage in the shortest time considering both instrument and communication constraints. We formally define this problem as:

Problem 1 (Communication-Aware Multi-Spacecraft Orbit Design) *Efficiently design a set of orbits around a small body (with irregular gravity field) for a set of small spacecraft with heterogeneous instruments, so as to maximize the amount of scientific data delivered to the carrier spacecraft over a prescribed time horizon. The spacecraft have no propulsion other than required to enter their initial orbit; each instrument can only collect data from regions of the body where instrument constraints (including sun angle, instrument range, and spacecraft view angle) are satisfied; spacecraft communicate according to a delay-tolerant networking framework and have limited on-board memory; and available communication bandwidth between the spacecraft depends on line-of-sight and distance between the spacecraft according to a known model.*

We remark that the problem formulation focuses on orbit optimization. Accordingly, we assume that shape model of the body is available as a triangular mesh, and that an accurate representation of its dynamical environment (e.g., a spherical harmonics parametrization of the gravity model) is available; we also neglect uncertainties in navigation and control of the spacecraft. In addition, we focus on efficient ground-based execution of our algorithms, and benchmark their performance on representative ground-based computing hardware.

We envision that the approach could also be used in receding-horizon fashion, using coarse shape and gravity models estimated from a safe distance, and gradually approaching the body as knowledge of its shape and dynamics improves; assessing the sensitivity of the proposed approach to uncertainty in the shape model and in the dynamical environment, and extending this work to on-orbit optimization, are key directions for future research.

III. A MILP formulation for simultaneous observation and relay optimization

In this section, we describe a mixed-integer linear programming (MILP)-based problem formulation that optimizes the observations collected by the spacecraft, and the inter-spacecraft communication activities, to maximize scientific returns for a *given* set of orbits. We also propose a linear programming (LP) relaxation of the optimization problem, and show that the gradient of the LP's objective function with respect to the spacecraft's initial conditions can be computed semi-analytically.

We consider a set \mathcal{A} of spacecraft orbiting a small body over a finite time period discretized by a set of time intervals $t \in \mathcal{T}$. All instantaneous quantities (e.g., the location of the spacecraft and the orientation of surface regions of the small body) are computed at the mid-point of the time intervals. The position of spacecraft $a \in \mathcal{A}$ along its orbit at time t is $\vec{x}_a(t) = \vec{x}_a(\mathcal{S}_a(t_0), t)$. Each spacecraft's orbit is parametrized by its initial state $\mathcal{S}_a(t_0) = (\vec{x}_a(t_0), \vec{v}_a(t_0))$ (or, equivalently, by its initial osculating orbital elements $(a_a(t_0), e_a(t_0), i_a(t_0), \Omega_a(t_0), \omega_a(t_0), \theta_a(t_0))$). Spacecraft are equipped with instruments in the set \mathcal{I} . Specifically, each spacecraft a is equipped with instrument i_a , and $\cup_{a \in \mathcal{A}} i_a = \mathcal{I}$. Multiple spacecraft may carry the same instrument; for simplicity, we consider the case where each spacecraft carries a single instrument.

It is of interest to observe a set of regions \mathcal{R} of the small body. The observability function $O : (\mathcal{R}, \mathcal{I}, \vec{x}, \mathcal{T}) \mapsto [0, 1]$ captures whether it is possible to observe region $r \in \mathcal{R}$ with instrument $i \in \mathcal{I}$ from location \vec{x} during time interval $t \in \mathcal{T}$, and the quality of the resulting observation. An observation with value 0 is infeasible or scientifically useless; an observation with value 1 is ideal. The observability function can encode a variety of geometric constraints including sun angle, spacecraft view angle, and ground resolution; Section III.A provides a formal description of the function and a discussion of relevant instrument constraints.

Observing region $r \in \mathcal{R}$ with instrument $i \in \mathcal{I}$ from location \vec{x} in time period $t \in \mathcal{T}$ yields a reward $U(r, i)O(r, i, \vec{x}, t)$ (which captures both the scientific interest of the region, through U , and the quality of the resulting data, through O) and produces an amount of data $D(r, i)$ which must be relayed to a carrier spacecraft. Spacecraft are able to communicate with each other through bandwidth-limited links. A bandwidth function $B : (\vec{x}_1, \vec{x}_2, \mathcal{T}) \mapsto \mathbb{R}$ denotes the available bandwidth between two spacecraft at locations \vec{x}_1 and \vec{x}_2 during time period $t \in \mathcal{T}$. Spacecraft can also store their own data or other spacecraft's data on board and forward it at a later time. Each spacecraft has a limited amount of memory aM . A spacecraft $c \in \mathcal{A}$ is denoted as the *carrier*. The goal of the problem is to maximize the amount of scientific data, weighted by the reward U and by the data quality O , that is collected by the spacecraft and delivered to the carrier.

Before we formally present the MILP model, we must define the observability and bandwidth functions.

A. Observability Function

We consider a differentiable observability function that captures the sun angle, view angle, and spacecraft-to-region range for each region, spacecraft, and instrument. Each region $r \in \mathcal{R}$ on the surface of the asteroid is characterized by a centroid \vec{x}_r and a unit normal vector \vec{n}_r perpendicular to the local surface of the region. We define the vector from the origin of the selected reference frame to the Sun position at the mid-point of time interval t as $\vec{x}_\odot(t)$.

We define the sun angle, view angle, and spacecraft-to-region range as follows, where $\|\cdot\|$ represents the ℓ^2 -norm:

$$\begin{aligned} \text{Sun angle } \hat{s}_\odot(r, t) &= \arccos(\vec{n}_r(t) \cdot (\vec{x}_\odot(t) - \vec{x}_r(t)) / (\|\vec{x}_\odot(t) - \vec{x}_r(t)\|)) \\ \text{View angle } \hat{s}_a(r, t) &= \arccos(\vec{n}_r(t) \cdot (\vec{x}_a(t) - \vec{x}_r(t)) / (\|\vec{x}_a(t) - \vec{x}_r(t)\|)) \\ \text{Spacecraft-to-region range } d_a(r, t) &= \|\vec{x}_a(t) - \vec{x}_r(t)\| \end{aligned}$$

The sun angle captures the angle between the local normal and the direction of the Sun, and therefore characterizes the illumination of the region; the view angle captures the angle at which an instrument on the spacecraft can observe the surface of the region; and the spacecraft-to-region range is simply the distance between the spacecraft and the centroid of the region.

For each instrument, the sun angle, view angle, and spacecraft-to-region range should lie within lower and upper bounds prescribed by science requirements determined on the basis of the science traceability matrix (STM). Table

1 reports a STM for a notional mission to 433 Eros, and the resulting constraints on sun angle, view angle, and spacecraft-to-region range. The STM, science payloads, and requirements are broadly inspired by the NEAR Shoemaker [6] and Dawn [7] missions, and in line with recent work on multi-spacecraft exploration of small bodies [8–10].

In order to capture the sensitivity of observability to the spacecraft’ orbits, we use a logistic function to enforce the upper and lower bounds. We recall that the logistic function is defined as $L(x) = \exp(x)/(1 + \exp(x))$. For a given upper bound \bar{x} , lower bound \underline{x} , and tolerance \tilde{x} , we define the *logistic window function* as

$$W(x, \bar{x}, \underline{x}, \tilde{x}) = L\left(\frac{x - \underline{x}}{\tilde{x}}\right) \left(1 - L\left(\frac{x - \bar{x}}{\tilde{x}}\right)\right) \quad (1)$$

The function $W(x, \bar{x}, \underline{x}, \tilde{x})$ assumes values close to 1 between \underline{x} and \bar{x} , and values close to 0 below \underline{x} and above \bar{x} . Figure 3 shows an example of the logistic window function.

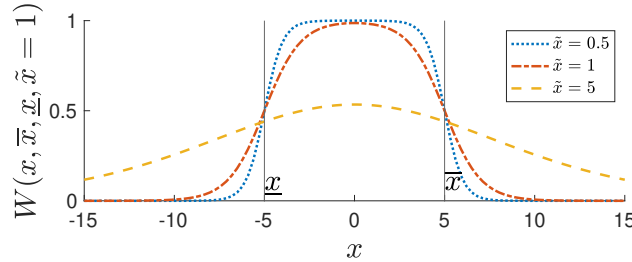


Fig. 3 Differentiable window function $W(x, \bar{x}, \underline{x}, \tilde{x})$ for $\bar{x} = 5, \underline{x} = -5$.

The tolerance parameter \tilde{x} plays a key role in the definition of the requirements. From a scientific standpoint, the parameter encodes how sensitive the science objective is to variations of the variable under consideration (e.g., the extent to which a change in view angle or sun angle improves, or worsens, the quality of the resulting data products). From an engineering standpoint, a larger parameter allows the optimization process to venture closer to the limits \underline{x} and \bar{x} with little reduction in reward, resulting in a larger feasible region; however, a large parameter also results in a flatter gradient far from the limit, which is less informative for the optimizer, and a steeper gradient close to the limits, which can introduce numerical convergence challenges.

We denote the maximum and minimum sun angle, view angle, and spacecraft-to-region ranges for an instrument i as $\bar{s}_{\odot}^i, \underline{s}_{\odot}^i, \bar{s}_a^i, \underline{s}_a^i, \bar{d}_a^i$, and \underline{d}_a^i respectively. We also denote the tolerances with respect to the sun angle, view angle, and spacecraft-to-region ranges as $\tilde{s}_{\odot}^i, \tilde{s}_a^i$, and \tilde{d}_a^i respectively.

We are now in a position to define the observability function as

$$O(r, i_a, \vec{x}_a(t), t) = W\left(\hat{s}_{\odot}(r, t), \bar{s}_{\odot}^{i_a}, \underline{s}_{\odot}^{i_a}, \tilde{s}_{\odot}^{i_a}\right) W\left(\hat{s}_a(r, t), \bar{s}_a^{i_a}, \underline{s}_a^{i_a}, \tilde{s}_a^{i_a}\right) W\left(d_a(r, t), \bar{d}_a^{i_a}, \underline{d}_a^{i_a}, \tilde{d}_a^{i_a}\right) \quad (2)$$

The observability function is close to one if the sun angle, view angle, and spacecraft-to-region range constraints

are all satisfied; if any one of the constraints is not satisfied, the function decreases to zero. We recall that, in the discrete-time formulation, instantaneous quantities (including observability) are computed at the mid-point of each time interval.

We remark that the proposed observability function does *not* capture the fact that some regions may be blocked from view by other parts of the small body (e.g., overhangs). The function could be readily updated with an additional term capturing view obstructions; however, such a formulation would introduce a non-differentiable discontinuity in the observability function, which could present a challenge to the gradient-based optimizer. We empirically observed that view obstructions not a major concern for the mission concept under consideration, as points that would be blocked from view by 433 Eros typically present poor observability because of their sun angle and view angle.

We assume that, at each time step, the spacecraft can choose to observe any one region with observability higher than a minimum threshold (selected by mission scientists), effectively abstracting away the spacecraft’s attitude control and pointing problem between time steps — a reasonable assumption if the time steps considered in the optimization are of sufficiently long duration, e.g., multiple minutes. Explicitly capturing attitude and slewing constraints is an interesting direction for future research.

B. Communication bandwidth

We model the available communication bandwidth between every pair of spacecraft in absence of obstructions as a quadratic function with an upper bound. The model is justified by the assumptions that (i) the radio signal between every pair of spacecraft is only subject to free-path loss (hence, the received signal power decreases quadratically with inter-spacecraft distance); (ii) the spacecraft are equipped with omnidirectional antennas; (iii) the noise at the receiver is approximately constant; and (iv) an adaptive encoding scheme is available that changes the available data transmission rate to adapt to the SNR available at the receiver. Formally, we define the free-space bandwidth as

$$B_{\text{fs}}(a_1, a_2, t) = \min \left(\bar{B}, B_0 \cdot \left(\frac{d_0}{\|\vec{x}_{a_1}(t) - \vec{x}_{a_2}(t)\|} \right)^2 \right), \quad (3)$$

where \bar{B} is the maximum bandwidth between every pair of spacecraft (a function of the encoding scheme used), B_0 is a reference bandwidth, and d_0 is the distance at which the selected radios, antennas, and encoding scheme can achieve the reference bandwidth B_0 .

We use a simple and conservative model to capture the effect of occlusions by the small body. For the purposes of communications, the asteroid is modeled by an outer sphere and an inner sphere, both centered at the asteroid’s center of mass, characterized by an outer radius $r_{\text{max},co}$ and an inner radius $r_{\text{min},co}$ respectively. If the line-of-sight path between two spacecraft lies entirely outside the external sphere, the bandwidth is assumed to be the free-space bandwidth B_{fs} . If the line-of-sight path intersects the inner sphere, the bandwidth is assumed to be 0. If the free-space

path intersects the outer sphere but not the inner sphere, the bandwidth is reduced proportionally to the closest distance between the free-space path and the center of the spheres.

The two-sphere model is less accurate than a ray-traced occlusion model for irregularly-shaped bodies; however, compared to higher-fidelity models, it offers the key advantage of *differentiability*. By providing a region where inter-spacecraft bandwidth decreases but does not immediately vanish, and by offering an analytical expression for the gradient of bandwidth with respect to the spacecraft positions, the two-sphere model provides the gradient-based optimizer a useful clue to nudge orbits away from occlusions, allowing the optimizer to avoid them - a property that is discussed further in Section IV.B.

Formally, the distance between the closest point on the line-of-sight path between spacecraft a_1 and a_2 and the small body's center of mass \vec{x}_{cg} can be computed as

$$\underline{d}(a_1, a_2, t) = \min \left(\begin{array}{l} \|\vec{x}_{a_1}(t) - \vec{x}_{cg}\|, \|\vec{x}_{a_2}(t) - \vec{x}_{cg}\|, \\ \sqrt{\|\vec{x}_{a_1}(t) - \vec{x}_{cg}\|^2 - [(\vec{x}_{a_2}(t) - \vec{x}_{a_1}(t)) \cdot (\vec{x}_{a_1}(t) - \vec{x}_{cg})]^2 / \|\vec{x}_{a_2}(t) - \vec{x}_{a_1}(t)\|^2} \end{array} \right) \quad (4)$$

where the first and second expression correspond to the cases where spacecraft a_1 or a_2 are the closest points to the center of mass on the line-of-sight segment, and the third expression is the distance between the line connecting the two spacecraft and the body's center of mass.

The level of communication obstruction between two spacecraft is then defined as

$$CO(a_1, a_2, t) = 1 - \min \left(1, \max \left(0, \frac{\underline{d}(a_1, a_2, t) - r_{min,co}}{r_{max,co} - r_{min,co}} \right) \right), \quad (5)$$

and the bandwidth between the two spacecraft is

$$B(a_1, a_2, t) = B_{fs}(a_1, a_2, t)(1 - CO(a_1, a_2, t)) \quad (6)$$

Remarks Some remarks on the communication model are in order. The communication model makes several strong assumptions, chiefly (i) quadratic loss model for the transmitted signal, (ii) availability of a perfect adaptive encoding scheme, (iii) availability of omnidirectional antennas, (iv) neglecting interference between multiple spacecraft and (iv) simple (but conservative) modeling of obstructions. We argue that such a model is appropriate to capture the availability of communication bandwidth for *system-level design* of a multi-spacecraft swarm; in particular, in exchange for somewhat reduced fidelity, the proposed model provides analytical insight into how changes in each spacecraft's orbit affect available bandwidth, as discussed in Section IV. More accurate communication models can then be used in *simulation* to validate the performance of the selected design and, if needed, refine the communication model. Two

assumptions merit further discussion. First, the assumption that interference between the spacecraft is negligible is comparatively realistic if spacecraft use a time-division or frequency-division multiple access scheme to share the wireless medium; future work will address the inclusion of other adaptive multiple-access schemes. Second, the assumption that a perfect adaptive encoding scheme is available is a *continuous approximation* of existing adaptive encoding schemes that increase and decrease the transmitted symbol rate based on sensed signal-to-noise ratio, which are widely supported in terrestrial communication protocols such as 802.11 [22, 23].

C. A mixed-integer linear programming formulation

We are now in a position to define the *communication-aware observation scheduling problem*.

Problem 2 (Communication-aware observation scheduling problem) *Select the observations collected by the spacecraft and the inter-spacecraft data flows so as to maximize the reward for observations captured and delivered to the carrier, while satisfying bandwidth constraints on inter-spacecraft links and memory constraints on board each spacecraft.*

We pose the problem as a mixed-integer linear program. Specifically, we describe observations as binary variables that are true if and only if a given agent observes a given region at a given time, and we model data transfers between the spacecraft with a network flow formulation [24]. In the network flow formulation, the communication problem is modeled as a graph where every node represents a spacecraft at a given discrete time step; edges between pairs of spacecraft represent the availability of a communication link (with an upper bound on the amount of data that can be transmitted between the spacecraft due to available bandwidth); edges between nodes representing the same spacecraft at different time steps represent the availability of on-board memory (with an upper bound capturing the overall amount of available memory); data sources correspond to the observations; and the carrier spacecraft acts as a sink for information flow. Figure 4 provides a graphical representation of the network flow communication model. We refer the interested reader to [24] for a review of network flow formulations and their application to communication problems.

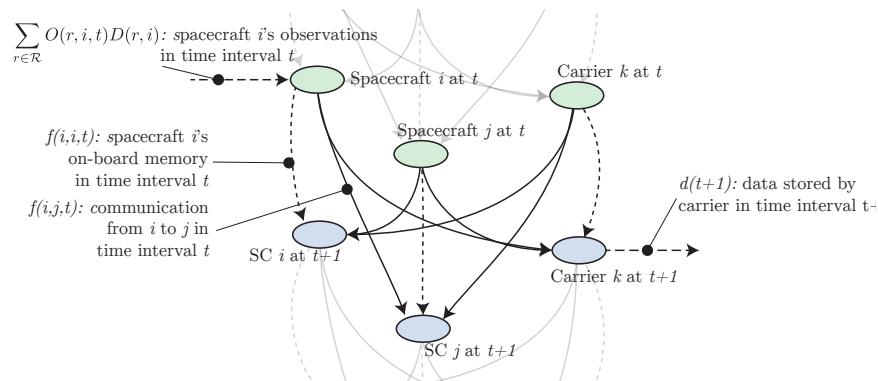


Fig. 4 Network flow model for inter-spacecraft communication.

Variables We define the following variables.

- $p : (\mathcal{R}, \mathcal{A}, \mathcal{T}) \mapsto \{0, 1\}$ is a Boolean-valued variable that assumes value 1 iff the instrument of agent $a \in \mathcal{A}$ points at region $r \in \mathcal{R}$ during time interval $t \in \mathcal{T}$.
- $o : (\mathcal{R}, \mathcal{A}, \mathcal{T}) \mapsto [0, 1]$ is a real-valued variable that denotes the fraction of region $r \in \mathcal{R}$ that is observed by agent $a \in \mathcal{A}$ during time interval $t \in \mathcal{T}$. While we assume that a spacecraft can observe the entirety of a region in one time step, it may be desirable to allow the spacecraft to only store and forward data from a *fraction* of the region (rather than skipping the observation entirely) if insufficient storage or communication bandwidth is available.
- $f : (\mathcal{A}, \mathcal{A}, \mathcal{T}) \mapsto \mathbb{R}^+$ is a real-valued variable that denotes the amount of data transmitted from agent $a_1 \in \mathcal{A}$ to agent $a_2 \in \mathcal{A}$ during time interval $t \in \mathcal{T}$. If $a_1 = a_2$, the variable denotes the amount of data in agent $a_1 = a_2$'s memory during time interval t .
- $d : \mathcal{T} \mapsto \mathbb{R}^+$ is a real-valued variable that denotes the amount of data received and stored by the carrier during time interval $t \in \mathcal{T}$.

Problem Formulation We formalize the *Communication-aware observation scheduling problem* problem as follows.

$$\max_{p,o,f,d} \sum_{a \in \mathcal{A}} \sum_{r \in \mathcal{R}} \sum_{t \in \mathcal{T}} o(r, a, t) \cdot U(r, i_a) \cdot O(r, i_a, \vec{x}_a(t), t) \quad (7a)$$

subject to

$$\sum_{t \in \mathcal{T}} \sum_{a \in \mathcal{A}} o(r, a, t) \leq 1 \quad \forall r \in \mathcal{R} \quad (7b)$$

$$o(r, a, t) \leq p(r, a, t) \quad \forall r \in \mathcal{R}, a \in \mathcal{A}, t \in \mathcal{T} \quad (7c)$$

$$\sum_{r \in \mathcal{R}} p(r, a, t) \leq 1 \quad \forall a \in \mathcal{A}, t \in \mathcal{T} \quad (7d)$$

$$\sum_{r \in \mathcal{R}} (o(r, a, t)D(r, a)) + \mathbf{1}_{t \neq \min(\mathcal{T})} \sum_{a_- \in \mathcal{A}} f(a_-, a, t-1) = \mathbf{1}_{t \neq \max(\mathcal{T})} \sum_{a_+ \in \mathcal{A}} f(a, a_+, t) + \mathbf{1}_{a=c}d(t) \quad \forall a \in \mathcal{A}, t \in \mathcal{T} \quad (7e)$$

$$f(a_1, a_2, t) \leq B(a, b, t) \quad \forall a_1 \in \mathcal{A}, a_2 \neq a_1 \in \mathcal{A}, t \in \mathcal{T} \quad (7f)$$

$$f(a, a, t) \leq M_a \quad \forall a \in \mathcal{A}, t \in \mathcal{T} \quad (7g)$$

$$f(a_1, a_2, t_0) = 0 \quad \forall a_1 \in \mathcal{A}, a_2 \in \mathcal{A} \quad (7h)$$

$$p(r, a, t) \in \{0, 1\} \quad \forall r \in \mathcal{R}, a \in \mathcal{A}, t \in \mathcal{T} \quad (7i)$$

Equation (7b) ensures that every region is observed at most once, including fractional observations. Equation (7c)

ensures that a region can only be observed by a spacecraft if the spacecraft is pointing towards it. Equation (7d) ensures that every agent points at at most one region per time step. Equation (7e) models data flows among the agents and ensures that data is only created when an observation is performed and data is only recorded at the carrier. Equation (7f) ensures that data flows on communication links do not exceed the available bandwidth, and Equation (7g) enforces the on-board memory capacity constraint. Finally, Equation (7h) sets the initial memory usage of the spacecraft and the initial data flows to zero, and Equation (7i) ensures that the observation variables assume binary values.

We remark that *all* data collected by the spacecraft must be delivered to the carrier, since the network flow formulation is conservative: that is, $\sum_{a \in \mathcal{A}} \sum_{t \in \mathcal{T}} \sum_{r \in \mathcal{R}} o(r, a, t) D(r, a) = \sum_{t \in \mathcal{T}} d(t)$. To see this, consider the sum of Equations (7e) over all $a \in \mathcal{A}, t \in \mathcal{T}$, and note that each of the flow terms $f(a_1, a_2, t)$ appear twice in the sum, with opposite signs, yielding the property above. This property allows to formulate the objective function in terms of the observations (which, in turn, allows to capture the importance and quality of observations through the functions U and O respectively), while ensuring that all collected data is delivered to the carrier.

D. A Linear Relaxation

Problem (7) can be solved efficiently by commercial MILP solvers. However, the MILP formulation does not provide analytical insight into the *sensitivity* of the problem to the problem parameters (namely, the observability function and the bandwidths). In contrast, we are interested in assessing how changes to these parameters (which are, in turn, connected to changes in the selected initial conditions) can affect the solution to Problem (7).

To overcome this, we consider a *linear relaxation* of Problem (7), where the Boolean-valued pointing variable p is replaced by a real-valued variable, and Equation (7i) is replaced by its linear relaxation. The resulting problem is:

$$\max_{o, f, d} \text{(7a)} \tag{8a}$$

subject to

$$\text{(7b), (7c), (7d), (7e), (7f), (7g) and (7h)} \tag{8b}$$

$$0 \leq p(r, a, t) \leq 1 \quad \forall r \in \mathcal{R}, a \in \mathcal{A}, t \in \mathcal{T} \tag{8c}$$

Next, we observe that the variable p only appears in Equations (7c), (7d), and (8c). If p is real-valued, one can show that the three equations can be replaced by $o(r, a, t) \leq 1$ and $0 \leq o(r, a, t) \leq 1$, with no loss of generality, and the variable p can be removed from the optimization problem entirely. The resulting linear program is

$$\max_{o, f, d} \sum_{a \in \mathcal{A}} \sum_{r \in \mathcal{R}} \sum_{t \in \mathcal{T}} o(r, a, t) \cdot U(r, i_a) \cdot O(r, i_a, \vec{x}_a(t), t) \tag{9a}$$

subject to

$$\sum_{t \in \mathcal{T}} \sum_{a \in \mathcal{A}} o(r, a, t) \leq 1 \quad \forall r \in \mathcal{R} \text{ with dual } \mu_r \quad (9b)$$

$$\sum_{r \in \mathcal{R}} o(r, a, t) \leq 1 \quad \forall a \in \mathcal{A}, t \in \mathcal{T} \text{ with dual } \mu_{a,t} \quad (9c)$$

$$\sum_{r \in \mathcal{R}} (o(r, a, t)D(r, a)) + \mathbf{1}_{t \neq \min(\mathcal{T})} \sum_{a_- \in \mathcal{A}} f(a_-, a, t-1) = \mathbf{1}_{t \neq \max(\mathcal{T})} \sum_{a_+ \in \mathcal{A}} f(a, a_+, t) + \mathbf{1}_{a=c} d(t) \quad \forall a \in \mathcal{A}, t \in \mathcal{T} \text{ with dual } \lambda_{a,t} \quad (9d)$$

$$f(a_1, a_2, t) \leq B(a, b, t) \quad \forall a_1 \in \mathcal{A}, a_2 \neq a_1 \in \mathcal{A}, t \in \mathcal{T} \text{ with dual } \mu_{a_1, a_2, t} \quad (9e)$$

$$f(a, a, t) \leq M_a \quad \forall a \in \mathcal{A}, t \in \mathcal{T} \text{ with dual } \mu_{a, a, t} \quad (9f)$$

$$f(a_1, a_2, t_0) = 0 \quad \forall a_1 \in \mathcal{A}, a_2 \in \mathcal{A} \quad (9g)$$

$$0 \leq o(r, a, t) \leq 1 \quad \forall r \in \mathcal{R}, a \in \mathcal{A}, t \in \mathcal{T} \quad (9h)$$

The key effect of the linear relaxation is that, at any given time step, a spacecraft may observe multiple regions, so long as the sum of the fractional observations is smaller than one.

This effect is highly problematic: allowing a spacecraft to observe multiple regions within the same time step would require it to slew to multiple points within a single time step, which is inconsistent with the problem formulation.

To ensure that, at every time step, every spacecraft observes a single region, we *post-process* the solution of Problem (9) to obtain a feasible solution to Problem (7) by setting to zero all but one of the variables o corresponding to a given agent and a given timestep.

In Section VI.A, we show through numerical simulations that the post-processing step generally results in a very small decrease in the objective function value compared to the LP relaxation (9). This suggests that, on the one hand, the post-processed solution is close to optimal (since the LP (9) provides an upper bound on the optimum, and the post-processed solution provides a lower bound); and, on the other hand, the LP relaxation is a *good proxy* for the post-processed solution, and, by extension, for the optimum, justifying its use for sensitivity analysis. Crucially, as discussed next, the LP relaxation also provides analytical insight into the sensitivity of the problem to its parameters; we will exploit this insight to efficiently explore the space of feasible initial conditions and maximize the objective function (7a).

IV. Sensitivity

In this section, we show how the gradient of the objective function of the LP relaxation (9) with respect to the spacecraft initial conditions $\{\mathcal{S}_a\}_{a \in \mathcal{A}}$ can be computed semi-analytically.

The only parameters of Problem (9) that are affected by the spacecraft orbits (and therefore by their initial locations) are the observation rewards U and the bandwidths B .

Let us denote the value of the objective function (7a) at the optimum as K^* , and the corresponding optimal value of the observation variables as o^* . We can express the gradient of K^* with respect to the spacecraft initial conditions $\{\mathcal{S}_a(t_0)\}_{a \in \mathcal{A}}$ as:

$$\begin{aligned} \frac{\partial K^*}{\partial \mathcal{S}_a} &= \sum_{r \in \mathcal{R}} \sum_{t \in \mathcal{T}} \left(\frac{\partial K^*}{\partial O(r, i_a, \vec{x}_a(t), t)} \cdot \frac{\partial O(r, i_a, \vec{x}_a(t), t)}{\partial \mathcal{S}_a(t_0)} \right) + \\ &\quad \sum_{t \in \mathcal{T}} \sum_{a_- \in \mathcal{A}} \left(\frac{\partial K^*}{\partial B(\vec{x}_{a_-}(t), \vec{x}_a(t), t)} \cdot \frac{\partial B(\vec{x}_{a_-}(t), \vec{x}_a(t), t)}{\partial \mathcal{S}_a(t_0)} \right) + \\ &\quad \sum_{t \in \mathcal{T}} \sum_{a_+ \in \mathcal{A}} \left(\frac{\partial K^*}{\partial B(\vec{x}_a(t), \vec{x}_{a_+}(t), t)} \cdot \frac{\partial B(\vec{x}_a(t), \vec{x}_{a_+}(t), t)}{\partial \mathcal{S}_a(t_0)} \right) \\ &= \sum_{r \in \mathcal{R}} \sum_{t \in \mathcal{T}} \left(\frac{\partial K^*}{\partial O(r, i_a, \vec{x}_a(t), t)} \cdot \frac{\partial O(r, i_a, \vec{x}_a(t), t)}{\partial \vec{x}_a(t)} \cdot \frac{\partial \vec{x}_a(t)}{\partial \mathcal{S}_a(t_0)} \right) + \\ &\quad \sum_{t \in \mathcal{T}} \sum_{a_- \in \mathcal{A}} \left(\frac{\partial K^*}{\partial B(\vec{x}_{a_-}(t), \vec{x}_a(t), t)} \cdot \frac{\partial B(\vec{x}_{a_-}(t), \vec{x}_a(t), t)}{\partial \vec{x}_a(t)} \cdot \frac{\partial \vec{x}_a(t)}{\partial \mathcal{S}_a(t_0)} \right) + \\ &\quad \sum_{t \in \mathcal{T}} \sum_{a_+ \in \mathcal{A}} \left(\frac{\partial K^*}{\partial B(\vec{x}_a(t), \vec{x}_{a_+}(t), t)} \cdot \frac{\partial B(\vec{x}_a(t), \vec{x}_{a_+}(t), t)}{\partial \vec{x}_a(t)} \cdot \frac{\partial \vec{x}_a(t)}{\partial \mathcal{S}_a(t_0)} \right). \end{aligned}$$

The derivative of the objective function K^* with respect to the bandwidth $B(\vec{x}_a(t), \vec{x}_{a_+}(t), t)$ evaluated at the optimum is $\mu_{a, a_+, t}$, by the definition of the dual. Likewise, the derivative of the objective function K^* with respect to the bandwidth $B(\vec{x}_{a_-}(t), \vec{x}_a(t), t)$ is $\mu_{a_-, a, t}$. The derivative of the objective function with respect to the observability function $O(r, i_a, \vec{x}_a(t), t)$ is simply $o^*(r, a, t)U(r, i_a)$, according to Equation (7a).

We recall that the sensitivity of a trajectory to its initial conditions is captured by the *state transition matrix* (STM) [25]:

$$\mathcal{S}_a(t) = \Phi_a(t, t_0) \mathcal{S}_a(t_0)$$

We denote the top three rows of the STM, representing the sensitivity of the position to the initial state, as $\Phi_a^x(t, t_0)$, and the bottom three rows of the STM, representing the sensitivity of the velocity, as $\Phi_a^v(t, t_0)$. Then,

$$\frac{\partial \vec{x}_a(t)}{\partial \mathcal{S}_a(t_0)} = \Phi_a^x(t, t_0) \quad \text{and} \quad \frac{\partial \vec{v}_a(t)}{\partial \mathcal{S}_a(t_0)} = \Phi_a^v(t, t_0) \quad (10)$$

Accordingly,

$$\begin{aligned} \frac{\partial K^*}{\partial \mathcal{S}_a} &= \sum_{r \in \mathcal{R}} \sum_{t \in \mathcal{T}} \left(o^*(r, a, t)U(r, i_a) \cdot \frac{\partial O(r, i_a, \vec{x}_a(t), t)}{\partial \vec{x}_a(t)} \cdot \Phi_a^x(t, t_0) \right) + \\ &\quad \sum_{t \in \mathcal{T}} \sum_{a_- \in \mathcal{A}} \left(\mu_{a_-, a, t} \cdot \frac{\partial B(\vec{x}_{a_-}(t), \vec{x}_a(t), t)}{\partial \vec{x}_a(t)} \cdot \Phi_a^x(t, t_0) \right) + \end{aligned}$$

$$\sum_{t \in \mathcal{T}} \sum_{a_+ \in \mathcal{A}} \left(\mu_{a, a_+, t} \cdot \frac{\partial B(\vec{x}_a(t), \vec{x}_{a_+}(t), t)}{\partial \vec{x}_a(t)} \cdot \Phi_a^x(t, t_0) \right) \quad (11)$$

The derivatives of the observability function (2) and of the bandwidths (6) can be computed analytically, as discussed next.

A. Gradient of the observability function

For ease of notation, let us call

$$\begin{aligned} W_{\odot}^i(\hat{s}_{\odot}(r, t)) &= W(\hat{s}_{\odot}(r, t), \vec{s}_{\odot}^{i_a}, \underline{s}_{\odot}^{i_a}, \vec{s}_{\odot}^{i_a}); \\ W_{\hat{a}}^i(\hat{s}_a(r, t)) &= W(\hat{s}_a(r, t), \vec{s}_a^{i_a}, \underline{s}_a^{i_a}, \vec{s}_a^{i_a}); \\ W_d^i(d_a(r, t)) &= W(d_a(r, t), \vec{d}_a^{i_a}, \underline{d}_a^{i_a}, \vec{d}_a^{i_a}). \end{aligned}$$

The gradient of the observability function (2) with respect to the location of the corresponding agent is

$$\frac{\partial O(r, i_a, \vec{x}_a(t), t)}{\partial \vec{x}_a(t)} = W_{\odot}^i(\hat{s}_{\odot}(r, t)) \left(\frac{\partial W_{\hat{a}}^i(\hat{s}_a(r, t))}{\partial \vec{x}_a(t)} W_d^i(d_a(r, t)) + W_{\hat{a}}^i(\hat{s}_a(r, t)) \frac{\partial W_d^i(d_a(r, t))}{\partial \vec{x}_a(t)} \right).$$

Recall that the derivative of the logistic function is

$$\frac{\partial L((x - \underline{x})/\bar{x})}{\partial x} = L((x - \underline{x})/\bar{x}) (1 - L((x - \underline{x})/\bar{x})) / \bar{x}.$$

The derivative of a generic logistic window function $W(f(\vec{x}_a(t)), \bar{f}, \underline{f}, \tilde{f})$ (defined in (1)) can then be computed as

$$\frac{\partial W(f(\vec{x}_a(t)), \bar{f}, \underline{f}, \tilde{f})}{\partial \vec{x}_a(t)} = \left(\frac{\partial L((f - \underline{f})/\tilde{f})}{\partial f} (1 - L((f - \bar{f})/\tilde{f})) - L((f - \underline{f})/\tilde{f}) \frac{\partial L((f - \bar{f})/\tilde{f})}{\partial f} \right) \frac{\partial f(\vec{x}_a(t))}{\partial \vec{x}_a(t)}. \quad (12)$$

Finally, the gradient of the view angle with respect to the spacecraft position can be computed as

$$\frac{\partial \hat{s}_a(r, t)}{\partial \vec{x}_a(t)} = - \left(1 - \left(\frac{(\vec{x}_a(t) \cdot \vec{x}_r(t))}{\|\vec{x}_a(t)\| \|\vec{x}_r(t)\|} \right)^2 \right)^{-\frac{1}{2}} \left[\left(\frac{\vec{x}_a(t)}{\|\vec{x}_a(t)\|^3} \frac{1}{\|\vec{x}_r(t)\|} (\vec{x}_a(t) \cdot \vec{x}_r(t)) \right) + \frac{\vec{x}_r(t)}{\|\vec{x}_a(t)\| \|\vec{x}_r(t)\|} \right],$$

and the gradient of the spacecraft-to-region range with respect to the spacecraft position is simply

$$\frac{\partial d_a(r, t)}{\partial \vec{x}_a(t)} = \frac{\vec{x}_a(t) - \vec{x}_r(t)}{\|\vec{x}_a(t) - \vec{x}_r(t)\|}. \quad (13)$$

Accordingly, we can compute

$$\frac{\partial O(r, i_a, \vec{x}_a(t), t)}{\partial \vec{x}_a(t)} = W_{\odot}^i(\hat{s}_{\odot}(r, t)) \cdot \left[- \left(\frac{\partial L((\hat{s}_a - \underline{s}_a^{i_a})/\vec{s}_a^{i_a})}{\partial \hat{s}_a} (1 - L((\hat{s}_a - \vec{s}_a^{i_a})/\vec{s}_a^{i_a})) - L((\hat{s}_a - \underline{s}_a^{i_a})/\vec{s}_a^{i_a}) \frac{\partial L((\hat{s}_a - \vec{s}_a^{i_a})/\vec{s}_a^{i_a})}{\partial \hat{s}_a} \right) \right].$$

$$\left(1 - \left(\frac{(\vec{x}_a(t) \cdot \vec{x}_r(t))}{\|\vec{x}_a(t)\| \|\vec{x}_r(t)\|}\right)^2\right)^{-\frac{1}{2}} \left[\left(\frac{\vec{x}_a(t)}{\|\vec{x}_a(t)\|^3} \frac{1}{\|\vec{x}_r(t)\|} (\vec{x}_a(t) \cdot \vec{x}_r(t))\right) + \frac{\vec{x}_r(t)}{\|\vec{x}_a(t)\| \|\vec{x}_r(t)\|} \right] \cdot W_d^i(d_a(r, t)) + W_a^i(\hat{s}_a(r, t)) \left[\frac{\partial L((d_a - \underline{d}_a^i)/\bar{d}_a^i)}{\partial d_a} (1 - L((d_a - \bar{d}_a^i)/\bar{d}_a^i)) - L((d_a - \underline{d}_a^i)/\bar{d}_a^i) \frac{\partial L((d_a - \bar{d}_a^i)/\bar{d}_a^i)}{\partial d_a} \right] \frac{\vec{x}_a(t) - \vec{x}_r(t)}{\|\vec{x}_a(t) - \vec{x}_r(t)\|} \Big].$$

B. Gradient of the bandwidth function

The gradient of the bandwidth function (6) can be expressed as

$$\frac{\partial B(a_1, a_2, t)}{\partial \vec{x}_{a_1}(t)} = \frac{\partial B_{fs}(a_1, a_2, t)}{\partial \vec{x}_{a_1}(t)} (1 - CO(a_1, a_2, t)) - B_{fs}(a_1, a_2, t) \frac{\partial CO(a_1, a_2, t)}{\partial \vec{x}_{a_1}(t)}.$$

The derivative of the free-space bandwidth is

$$\frac{\partial B_{fs}(a_1, a_2, t)}{\partial \vec{x}_{a_1}(t)} = \begin{cases} -2B_0 \left(\frac{d_0}{\|\vec{x}_{a_2}(t) - \vec{x}_{a_1}(t)\|^2} \right)^2 \cdot (\vec{x}_{a_2}(t) - \vec{x}_{a_1}(t)) & \text{if } B_{fs} < \bar{B} \\ \vec{0} & \text{if } B_{fs} = \bar{B} \end{cases},$$

$$\frac{\partial B_{fs}(a_1, a_2, t)}{\partial \vec{x}_{a_2}(t)} = - \frac{\partial B_{fs}(a_1, a_2, t)}{\partial \vec{x}_{a_1}(t)},$$

and the derivative of the communication obstruction is

$$\frac{\partial CO(a_1, a_2, t)}{\partial \vec{x}_{a_{1,2}}(t)} = \begin{cases} -\frac{1}{r_{max,co} - r_{min,co}} \frac{\partial d(a_1, a_2, t)}{\partial \vec{x}_{a_{1,2}}(t)} & \text{if } r_{min,co} < \underline{d}(a_1, a_2, t) < r_{max,co} \\ \vec{0} & \text{if } \underline{d}(a_1, a_2, t) < r_{min,co} \text{ or } \underline{d}(a_1, a_2, t) > r_{max,co} \\ \text{undefined} & \text{if } \underline{d}(a_1, a_2, t) = r_{max,co} \text{ or } \underline{d}(a_1, a_2, t) = r_{min,co} \end{cases}$$

Finally, the derivative of the distance between the shortest-path segment from spacecraft a_1 to a_2 can be computed

as:

$$\frac{\partial d(a_1, a_2, t)}{\partial \vec{x}_{a_1}(t)} = \begin{cases} (\vec{x}_{a_1}(t) - \vec{x}_{cg}) / \|\vec{x}_{a_1}(t) - \vec{x}_{cg}\| & \text{if } \underline{d}(a_1, a_2, t) = \|\vec{x}_{a_1}(t) - \vec{x}_{cg}\| \\ \vec{0} & \text{if } \underline{d}(a_1, a_2, t) = \|\vec{x}_{a_2}(t) - \vec{x}_{cg}\| \\ 1/2 \left\{ 2(\vec{x}_{a_1} - \vec{x}_{cg}) - \left[2(\vec{x}_{a_2} - \vec{x}_{a_1}) \cdot (\vec{x}_{a_1} - \vec{x}_{cg}) \right. \right. \\ \left. \left. (\vec{x}_{a_2} - 2\vec{x}_{a_1} + \vec{x}_{cg}) \|\vec{x}_{a_2} - \vec{x}_{a_1}\|^2 \right. \right. \\ \left. \left. + 2((\vec{x}_{a_2} - \vec{x}_{a_1}) \cdot (\vec{x}_{a_1} - \vec{x}_{cg}))^2 (\vec{x}_{a_2} - \vec{x}_{a_1}) \right] \right. \\ \left. / \|\vec{x}_{a_2} - \vec{x}_{a_1}\|^4 \right\} / \underline{d}(a_1, a_2, t) & \text{otherwise} \end{cases}$$

and

$$\frac{\partial \underline{d}(a_1, a_2, t)}{\partial \vec{x}_{a_2}(t)} = \begin{cases} (\vec{x}_{a_2}(t) - \vec{x}_{cg}) / \|\vec{x}_{a_2}(t) - \vec{x}_{cg}\| & \text{if } \underline{d}(a_1, a_2, t) = \|\vec{x}_{a_2}(t) - \vec{x}_{cg}\| \\ \vec{0} & \text{if } \underline{d}(a_1, a_2, t) = \|\vec{x}_{a_1}(t) - \vec{x}_{cg}\| \\ -1/2 \left\{ \begin{aligned} & 2 (\vec{x}_{a_2} - \vec{x}_{a_1}) \cdot (\vec{x}_{a_1} - \vec{x}_{cg}) (\vec{x}_{a_1} - \vec{x}_{cg}) \\ & \|\vec{x}_{a_2} - \vec{x}_{a_1}\|^2 - 2 ((\vec{x}_{a_2} - \vec{x}_{a_1}) \cdot (\vec{x}_{a_1} - \vec{x}_{cg}))^2 \\ & (\vec{x}_{a_2} - \vec{x}_{a_1}) \cdot (\vec{x}_{a_2} - \vec{x}_{a_1}) / \|\vec{x}_{a_2} - \vec{x}_{a_1}\|^4 \end{aligned} \right\} / \underline{d}(a_1, a_2, t) & \text{otherwise} \end{cases}$$

Remark The derivative of the bandwidth with respect to the spacecraft locations is undefined whenever $\underline{d}(a_1, a_2, t) = r_{max,co}$ or $\underline{d}(a_1, a_2, t) = r_{min,co}$. However, the set of points where the derivative is undefined has measure zero; accordingly, the likelihood that the undefined derivative will be encountered in execution is vanishingly low. Future work will consider using smoother transition functions in Equations (6) and (5) to side-step the issue altogether.

C. Putting it all together

We are now in a position to evaluate the gradient (11). The primal and dual variables $o^*(r, a, t)$ and $\mu_{a-,a,t}$ are computed numerically by the LP solver when solving Problem (7). The state transition matrix Φ_a^x , in turn, is computed numerically by the trajectory integrator. Finally, the derivative of the observation reward function $U(r, i, \vec{x}_a, t)$ and bandwidth function $B(\vec{x}_{a_1}, \vec{x}_{a_2}, t)$ with respect to the agent position \vec{x}_a can be computed analytically, as discussed in Sections IV.A and IV.B respectively. Hence, the gradient (11) can be computed numerically with negligible numerical overhead.

V. Orbit optimization

Next, we turn our attention to the solution of Problem 1, i.e., selecting the set of initial conditions for the spacecraft that (approximately) maximizes the amount of science collected and delivered to the carrier. The problem is highly nonlinear; further, the irregular structure of the gravity field around small bodies makes it hard to gain analytical insight that could reduce the size of the search space.

In the light of this, we turn our attention to global numerical optimization techniques; specifically, we advocate for the use of a *multi-start gradient-based optimization* scheme. In the proposed scheme, a number of collision-free initial conditions are sampled for the set of spacecraft. Initial conditions that result in a collision with the asteroid, or stray too far from its sphere of influence, are rejected. Next, for each set of collision-free initial conditions, a gradient-based trust region algorithm [26, 27] locally optimizes the initial conditions by following the numerical gradient computed in (11), until it converges to a local minimum. Intuitively, the trust region algorithm repeatedly optimizes a linearized version of the problem by following the gradient within a “trust region” around the linearization, which captures the portion of the

state space where the linearized model is a good approximation of the full model. Critically, after each optimization step, the trust region is updated; the radius of the trust region is reduced if the optimization resulted in worse-than-predicted improvement in the reward function (suggesting that the gradient is a poor approximation of the underlying function), and the radius is increased if the gradient step results in better-than-predicted improvement (suggesting that the gradient is a good local approximation). The best local minimum found across all sampled sets of orbits is then returned.

Constraints on spacecraft orbits We augment the formulation to impose “soft” differentiable constraints on inter-spacecraft distances, on the maximum and minimum distance between the spacecraft and the small body, and on the spacecraft’ maximum and minimum velocity, through logistic window functions (1). Limits on the range between the spacecraft and the small body are typically motivated by orbit stability considerations; limits on the spacecraft’s velocity, together with the range limits, indirectly constrain the energy of the orbits that can be selected by the optimizer, and can also help speed up numerical convergence. The key motivation driving the selection of the logistic window functions (as opposed to “hard” binary constraints) is the desire to preserve *differentiability* of the problem, ensuring that a gradient-based optimizer can efficiently find locally-optimal sets of spacecraft orbits.

Let us denote the maximum and minimum allowed distance between each spacecraft and the small body’s center of mass as \bar{d}_a^{cg} and \underline{d}_a^{cg} , with tolerance \tilde{d}_a^{cg} ; and the maximum and minimum allowed spacecraft velocity \bar{v}_a and \underline{v}_a respectively, with tolerance \tilde{v}_a . To enforce the distance and speed constraints, we add the following term to the reward function (9a):

$$K_O = M_O \sum_{a \in \mathcal{A}} \sum_{t \in \mathcal{T}} \left[W \left(\|\bar{\mathbf{x}}_a(t) - \bar{\mathbf{x}}_{cg}\|, \bar{d}_a^{cg}, \underline{d}_a^{cg}, \tilde{d}_a^{cg} \right) + W \left(\|\bar{\mathbf{v}}_a(t)\|, \bar{v}_a, \underline{v}_a, \tilde{v}_a \right) \right] \quad (14)$$

where M_O is a large scalar value.

The expression (14) does *not* depend on the decision variables o , f , and d in Problem (9): accordingly, adding it to the cost function (9a) does not change the minimizer for a given set of orbits.

However, the *gradient* of (14) with respect to the spacecraft’ initial locations is nonzero, and can be computed as

$$\begin{aligned} \frac{\partial K_O}{\partial \mathcal{S}_a(t_0)} &= M_O \frac{\partial}{\partial \mathcal{S}_a(t_0)} \sum_{a \in \mathcal{A}} \sum_{t \in \mathcal{T}} \left[W \left(\|\bar{\mathbf{x}}_a(t) - \bar{\mathbf{x}}_{cg}\|, \bar{d}_a^{cg}, \underline{d}_a^{cg}, \tilde{d}_a^{cg} \right) + W \left(\|\bar{\mathbf{v}}_a(t)\|, \bar{v}_a, \underline{v}_a, \tilde{v}_a \right) \right] \quad (15) \\ &= M_O \sum_{t \in \mathcal{T}} \left[\frac{\partial W \left(\|\bar{\mathbf{x}}_a(t) - \bar{\mathbf{x}}_{cg}\|, \bar{d}_a^{cg}, \underline{d}_a^{cg}, \tilde{d}_a^{cg} \right)}{\partial \|\bar{\mathbf{x}}_a(t) - \bar{\mathbf{x}}_{cg}\|} \cdot \frac{\partial \|\bar{\mathbf{x}}_a(t) - \bar{\mathbf{x}}_{cg}\|}{\partial \bar{\mathbf{x}}_a(t)} \cdot \frac{\partial \bar{\mathbf{x}}_a(t)}{\partial \mathcal{S}_a(t_0)} + \frac{\partial W \left(\|\bar{\mathbf{v}}_a(t)\|, \bar{v}_a, \underline{v}_a, \tilde{v}_a \right)}{\partial \|\bar{\mathbf{v}}_a(t)\|} \cdot \frac{\partial \|\bar{\mathbf{v}}_a(t)\|}{\partial \bar{\mathbf{v}}_a(t)} \cdot \frac{\partial \bar{\mathbf{v}}_a(t)}{\partial \mathcal{S}_a(t_0)} \right] \end{aligned}$$

By substituting Equations (12), (13), and (10) in (15), we finally obtain

$$\begin{aligned} \frac{\partial K_O}{\partial \mathcal{S}_a(t_0)} &= M_O \sum_{t \in \mathcal{T}} \left[\left(\frac{\partial L((d - \underline{d}_a^{cg})/\tilde{d}_a^{cg})}{\partial d} \right) \Big|_{d=\|\bar{\mathbf{x}}_a(t) - \bar{\mathbf{x}}_{cg}\|} \left(1 - L \left(\frac{\|\bar{\mathbf{x}}_a(t) - \bar{\mathbf{x}}_{cg}\| - \bar{d}_a^{cg}}{\tilde{d}_a^{cg}} \right) \right) - \right. \\ &\quad \left. L \left(\frac{\|\bar{\mathbf{x}}_a(t) - \bar{\mathbf{x}}_{cg}\| - \underline{d}_a^{cg}}{\tilde{d}_a^{cg}} \right) \frac{\partial L((d - \bar{d}_a^{cg})/\tilde{d}_a^{cg})}{\partial d} \right] \Big|_{d=\|\bar{\mathbf{x}}_a(t) - \bar{\mathbf{x}}_{cg}\|} \cdot \frac{\bar{\mathbf{x}}_a(t) - \bar{\mathbf{x}}_{cg}}{\|\bar{\mathbf{x}}_a(t) - \bar{\mathbf{x}}_{cg}\|} \cdot \Phi_a^x(t, t_0) + \end{aligned}$$

$$\left(\frac{\partial L((v - \underline{v}_a)/\tilde{v}_a)}{\partial v} \Big|_{v=\|\tilde{v}_a\|} \left(1 - L\left(\frac{\|\tilde{v}_a\| - \underline{v}_a}{\tilde{v}_a}\right) \right) - L\left(\frac{\|\tilde{v}_a\| - \underline{v}_a}{\tilde{v}_a}\right) \frac{\partial L((v - \underline{v}_a)/\tilde{v}_a)}{\partial v} \Big|_{v=\|\tilde{v}_a\|} \right) \cdot \frac{\tilde{v}_a(t)}{\|\tilde{v}_a\|} \cdot \Phi_a^v(t, t_0) \Big] \quad (16)$$

Similarly, we constrain the inter-spacecraft distance to be larger than a lower bound \underline{d}_{isc} , in order to ensure collision avoidance between the spacecraft. To this end, we introduce the following reward term that pushes inter-spacecraft distances to be larger than the lower bound:

$$K_{isc} = M_{isc} \sum_{a_1 \in \mathcal{A}} \sum_{a_2 \in \{\mathcal{A} \setminus a_1\}} \sum_{t \in \mathcal{T}} L\left(\frac{\|\tilde{x}_{a_1}(t) - \tilde{x}_{a_2}(t)\| - \underline{d}_{isc}}{\tilde{d}_{isc}}\right). \quad (17)$$

Similar to Equation (14), Equation (17) does not depend on the decision variables o , f , and d , and therefore it does not affect the minimizer of Problem (9) for a given set of orbits. The gradient of Equation (17) can be computed as

$$\frac{\partial K_{isc}}{\partial \mathcal{S}_a(t_0)} = 2M_{isc} \sum_{a_2 \in \{\mathcal{A} \setminus a\}} \sum_{t \in \mathcal{T}} \left[\left(\frac{\partial L((d - \underline{d}_{isc})/\tilde{d}_{isc})}{\partial d} \Big|_{d=\|\tilde{x}_a(t) - \tilde{x}_{a_2}(t)\|} \right) \cdot \frac{\tilde{x}_a(t) - \tilde{x}_{a_2}(t)}{\|\tilde{x}_a(t) - \tilde{x}_{a_2}(t)\|} \cdot \Phi_a^x(t, t_0) \right] \quad (18)$$

By adding the reward functions (14) and (17) and their gradients (16) and (18) to Problem (9), we can ensure that the selected trajectories do not collide with each other and do not stray excessively far from the small body, with a minimal increase in computation cost compared to the original linear program.

We remark that careful selection of the constants M_O and M_{isc} and of the tolerances \tilde{d}_a^{cg} and \tilde{d}_{isc} is necessary to ensure that, on the one hand, the solution to the optimization problem satisfies the prescribed distance and velocity constraints; and, on the other hand, the gradient optimization algorithm is able to effectively explore the feasible search space. Intuitively, very large values of M_O and M_{isc} ensure that the distance and velocity constraints are satisfied, and small values for \tilde{d}_a^{cg} and \tilde{d}_{isc} make it possible for the optimizer to approach the boundaries of the feasible region; as $M_O, M_{isc} \rightarrow \infty$ and $\tilde{d}_a^{cg}, \tilde{d}_{isc} \rightarrow 0$, the behavior of the constraints (14) and (17) approaches that of “hard” constraints that allow all values between the lower and upper bound, and reject all values outside the window. However, overly small values for the tolerance parameters result in steep gradients near the boundaries of the feasible region, which can cause numerical convergence issues; and excessively large values for the constants can push the optimizer away from the boundaries of the feasible region, which can result in an overly constrained solution.

The global optimization process is summarized in Algorithm 1.

In Section VI, we show that the trust region algorithm explores the neighborhood of the sampled points quite effectively, resulting in significant improvements compared to the sampled initial conditions; however, the problem presents a number of local minima, hence the multi-start approach is essential to effectively explore the space of possible orbits.

Algorithm 1 Multi-start gradient based orbit optimization algorithm

```
1:  $\{\{\mathcal{S}_a^j(t_0)\}_{a \in \mathcal{A}}\}_{j \in [1, \dots, N]}$   $\leftarrow$  Sample  $N$  sets of feasible initial conditions for all spacecraft  $\mathcal{A}$ 
2: for  $j \in [1, \dots, N]$  do
3:    $K^{j\star}, \{\mathcal{S}_a(t_0)^{j\star}\}_{a \in \mathcal{A}} \leftarrow \text{TRUSTREGION}(\text{OPTIMIZEOBSERVATIONSANDCOMMS}(\{\mathcal{S}_a^j(t_0)\}_{a \in \mathcal{A}}))$   $\triangleright$  Find the set of
   orbits that optimize the reward returned by OPTIMIZEOBSERVATIONSANDCOMMS by following its gradient. Note that
   this will call the function OPTIMIZEOBSERVATIONSANDCOMMS multiple times.
4: end for
5:  $\text{best\_solution} \leftarrow \arg \max_{j \in [1, \dots, N]} K^{j\star}$ 
6: return  $\{\mathcal{S}_a(t_0)^{\text{best\_solution}, \star}\}_{a \in \mathcal{A}}$ 
7: function OPTIMIZEOBSERVATIONSANDCOMMS( $\{\mathcal{S}_a(t_0)\}_{a \in \mathcal{A}}$ ,  $\{U(r, i)\}_{r \in \mathcal{R}, i \in \mathcal{I}}$ )
8:   for  $a \in \mathcal{A}$  do
9:      $\{(\vec{x}_a(t), \vec{v}_a(t), \Phi_a^x(t, t_0), \Phi_a^v(t, t_0))\}_{t \in \mathcal{T}} \leftarrow \text{INTEGRATEORBIT}(\mathcal{S}_a(t_0))$ 
10:    if  $\{\vec{x}_a(t)\}_{t \in \mathcal{T}}$  in collision or too far from small body then
11:      return
12:    end if
13:  end for
14:   $\{B(a_1, a_2, t), \partial B / \partial \vec{x}_{a_1} t, \partial B / \partial \vec{x}_{a_2} t\}_{a_1, a_2 \in \mathcal{A}, t \in \mathcal{T}} \leftarrow \text{COMPUTE BANDWIDTH}(\{\vec{x}_a(t)\}_{t \in \mathcal{T}})_{a \in \mathcal{A}}$ 
15:   $\{O(r, i_a, \vec{x}_a(t), t), \partial O / \partial \vec{x}_a(t)\}_{r \in \mathcal{R}, i \in \mathcal{I}, a \in \mathcal{A}, t \in \mathcal{T}} \leftarrow \text{COMPUTE OBSERVABILITY}(\{\vec{x}_a(t)\}_{t \in \mathcal{T}})_{a \in \mathcal{A}}$ 
16:   $K^\star, o^\star, \{\mu_{a_1, a_2, t}\}_{a_1, a_2 \in \mathcal{A}, t \in \mathcal{T}} \leftarrow \text{SOLVE PROBLEM 9} (\{B(a_1, a_2, t)\}_{a_1, a_2 \in \mathcal{A}, t \in \mathcal{T}},$ 
   $\{O(r, i_a, \vec{x}_a(t), t)\}_{r \in \mathcal{R}, i \in \mathcal{I}, a \in \mathcal{A}, t \in \mathcal{T}}, \{U(r, i)\}_{r \in \mathcal{R}, i \in \mathcal{I}})$ 
17:   $\{\partial K^\star / \partial \mathcal{S}_a\}_{a \in \mathcal{A}} \leftarrow \text{COMPUTE GRADIENT 11} (o^\star, \{\mu_{a_1, a_2, t}\}_{a_1, a_2 \in \mathcal{A}, t \in \mathcal{T}}, \{\partial B(a_1, a_2, t) / \partial \vec{x}_{a_1} t\}_{a_1, a_2 \in \mathcal{A}, t \in \mathcal{T}},$ 
   $\{\partial B(a_1, a_2, t) / \partial \vec{x}_{a_2} t\}_{a_1, a_2 \in \mathcal{A}, t \in \mathcal{T}}, \{\partial O(r, i_a, \vec{x}_a(t), t) / \partial \vec{x}_a(t)\}_{r \in \mathcal{R}, i \in \mathcal{I}, a \in \mathcal{A}, t \in \mathcal{T}})$ 
18:   $K_O \leftarrow \text{EVALUATE EQUATION (14)}(\{(\vec{x}_a(t), \vec{v}_a(t))\}_{t \in \mathcal{T}})$ 
19:   $\{\partial K_O / \partial \mathcal{S}_a\}_{a \in \mathcal{A}} \leftarrow \text{EVALUATE EQUATION (16)}(\{(\vec{x}_a(t), \vec{v}_a(t)), \Phi_a^x(t, t_0), \Phi_a^v(t, t_0)\}_{t \in \mathcal{T}})$ 
20:   $K_{isc} \leftarrow \text{EVALUATE EQUATION (17)}(\{(\vec{x}_a(t), \vec{v}_a(t))\}_{t \in \mathcal{T}})$ 
21:   $\{\partial K_{isc} / \partial \mathcal{S}_a\}_{a \in \mathcal{A}} \leftarrow \text{EVALUATE EQUATION (18)}(\{(\vec{x}_a(t), \vec{v}_a(t)), \Phi_a^x(t, t_0)\}_{t \in \mathcal{T}})$ 
22:  return  $K^\star + K_O + K_{isc}, \{\partial K^\star / \partial \mathcal{S}_a + \partial K_O / \partial \mathcal{S}_a + \partial K_{isc} / \partial \mathcal{S}_a\}_{a \in \mathcal{A}}$ 
23: end function
```

Remarks A few comments are in order. First, the proposed global search technique is *not* guaranteed to find the global optimum of the problem; this is unsurprising, given the nonconvex nature of the problem and the potential presence of a multitude of local minima. We remark that a number of sophisticated gradient-based global search algorithms are available [28]; the application of such algorithms to effectively explore the space of feasible initial conditions is an interesting direction for future research. On the upside, the proposed technique enjoys the *anytime* property [29]: that is, it will return a feasible (but possibly suboptimal) solution if it is interrupted before convergence, so long as the sampled initial conditions are feasible. Furthermore, the approach is highly parallelizable: the sampling process in Algorithm 1 and the subsequent trust-region-based optimization can be executed in parallel for each sampled point. Therefore, the numerical performance of the the proposed approach scales linearly with the number of cores available for optimization.

Second, the proposed optimization scheme does not include constraints such as fuel consumption or ΔV budget; however, such constraints could readily be incorporated as nonlinear constraints in the trust region algorithm.

Third, we remark that the local trust-region based optimization holds promise for *online re-optimization* of existing orbits: by only considering the gradient of the orbit with respect to the initial velocity, one can compute impulsive maneuvers for one or multiple spacecraft to locally improve science returns. Applying the proposed approach to online

re-optimization is an interesting direction for future research.

Finally, we remark that the proposed optimization scheme does *not* guarantee that the computed orbits will be stable beyond the time horizon of consideration. This is a major limitation of the proposed approach, since the optimizer may select orbits that guarantee good science returns over the time horizon of interest, but result in a collision with the asteroid or in a spacecraft leaving the asteroid’s sphere of influence shortly thereafter. Analytical and numerical tools are available to assess the stability of orbits around small bodies [25]; the incorporation of such constraints in the global optimization algorithm is a critical direction for future research.

VI. Results

We assess the performance of the proposed approach on a notional mission to 433 Eros with multiple smallsats equipped with cameras, imaging and X-Ray spectrometers, and radio altimeters.

Specifically, we consider a system with six small satellites carrying two imaging spectrometers, two cameras, an X-Ray spectrometer, and an altimeter (in addition to a carrier spacecraft in a circular 100km orbit). The reward $U(r, i)$ associated with imaging spectrometer observations, X-Ray spectrometer observations, camera observations, and altimeter readings is 3, 2, 1, and 0.5 respectively. The available bandwidth is $B_0 = 10$ kbps at a reference distance $d_0 = 100$ km. Only regions with an observability higher than 0.25 are considered in the observation scheduling problem. The data rates and pointing requirements of the instruments are reported in Table 1.

First, we analyze the performance of the proposed approach for communication-aware observation scheduling (Problem 2); next, we turn our attention to the problem of communication-aware orbit optimization (Problem 1).

A. Communication-aware observation scheduling

The problem of communication-aware observation scheduling (Problem 2) is a critical subroutine in the proposed optimization framework. To assess its performance, we analyze the relationship between the LP relaxation (9), which represents a (possibly infeasible) upper bound on the reward of Problem (7), and the feasible, possibly suboptimal post-processed version. We also assess the computation time of Problem (9) on commodity computing hardware.

Comparison of LP, and post-processed solutions Figure 5 shows the ratio between the post-processed LP solution (which provides a feasible, suboptimal solution to Problem (7)) and the original solution to (9) (which provides a potentially infeasible upper bound) for 500 randomly-selected sets of initial conditions. The reference bandwidth b_0 is set to 10 kbps at 100 km, in line with the capabilities of current smallsat UHF radio links [30]. A 7-day time horizon and 10-minute time step are considered.

The results in Figure 5 show that the post-processing step only results in a small reduction in optimality: for 99.2% of the post-processed solutions, the objective functions falls within 2% of the LP solution’s value and, by extension,

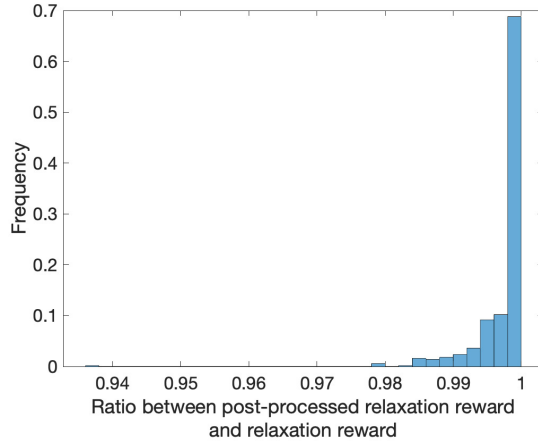


Fig. 5 Ratio between the reward of the post-processed LP relaxation and the original solution to Problem (9) for 500 randomly-selected configurations of seven spacecraft around 433 Eros.

of the optimum. Only a single simulation out of five hundred resulted in an objective value over 3% lower than the upper bound. These results suggest that it is appropriate to use Problem (9) as a proxy for the original Problem (7): the approach yields a solution with cost close to the optimum, with reliably fast computational times (as discussed in the next paragraph) and, crucially, it allows to efficiently assess the sensitivity of the problem to the problem parameters.

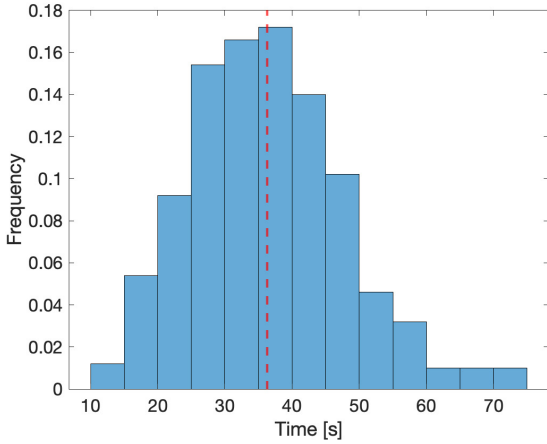
Computation times Figure 6 shows the time required to solve Problem (9) (left) and the overall time required to compute observability and bandwidths, solve the problem, and compute the gradient (right), for 500 randomly-selected configurations of a seven-spacecraft system around 433 Eros. A 7-day time horizon and 10-minute time step are considered. The problem is solved on a 10-core E5-2687W v3 Xeon workstation with 64 GBs of Ram. The Mosek LP solver is used.

The MATLAB implementation of the algorithm is not especially optimized for computational performance; nevertheless, even a large seven-spacecraft problem can be posed and solved in an average of 91.6s, and the time required to actually solve the optimization problem with the Mosek solver is on average 36.3s. These results show that the proposed approach can be executed in seconds to minutes on commodity desktop workstations, making it possible to effectively use it as the inner loop of a global search optimization scheme.

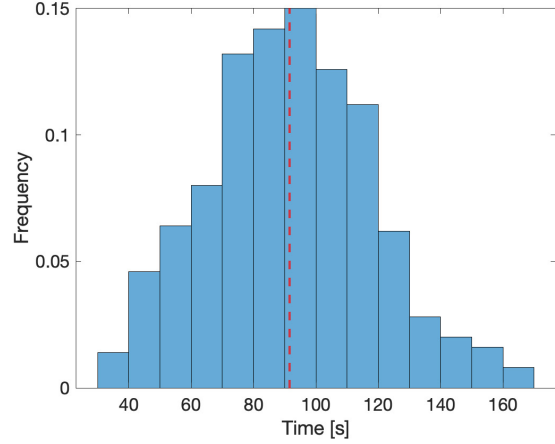
B. Communication-aware orbit optimization

Next, we turn our attention to the problem of communication-aware orbit optimization, and we assess the performance of Algorithm 1 compared to a communication-agnostic optimizer, and its computation time.

Comparison to a communication-agnostic optimizer We compare the effectiveness of the proposed communication-aware orbit optimizer with a communication-agnostic optimizer that first approximately optimizes the orbits to maximize



(a) Time required to solve Problem (9) to optimality.



(b) Time required to compute observability and bandwidths, solve Problem (9) to optimality, and compute the gradient.

Fig. 6 Computation time to solve Problem (9) for 500 randomly-selected configurations of seven spacecraft around 433 Eros.

the amount of data collected, and then solves Problem (9) to determine the amount of data that can be effectively delivered to the carrier.

The problem of optimizing a set of orbits to maximize the amount of data collected is itself nontrivial. To approximately solve it, we employ a greedy heuristic where, for every instrument type, the orbits of the spacecraft carrying the instrument are optimized sequentially; each orbit approximately maximizes the amount of new data points observed, while ensuring that no data point observed by previous spacecraft is observed a second time. To achieve this, for each spacecraft a and for a given set of initial conditions for the spacecraft, we solve a simplified version of Problem (7) where the communication constraints are ignored, namely

$$\max_{p,o,f,d} \sum_{r \in \mathcal{R}} \sum_{t \in \mathcal{T}} o(r, a, t) U(r, i_a) \cdot O(r, i_a, \vec{x}_a(t), t) \quad (19a)$$

subject to

$$\sum_{t \in \mathcal{T}} \sum_{\hat{a} \in \mathcal{A}} o(r, \hat{a}, t) \leq 1 \quad \forall r \in \mathcal{R} \quad (19b)$$

$$o(r, a, t) \leq p(r, a, t) \quad \forall r \in \mathcal{R}, a \in \mathcal{A}, t \in \mathcal{T} \quad (19c)$$

$$\sum_{r \in \mathcal{R}} p(r, a, t) \leq 1 \quad \forall t \in \mathcal{T} \quad (19d)$$

$$p(r, a, t) \in [0, 1] \quad \forall r \in \mathcal{R}, t \in \mathcal{T} \quad (19e)$$

When solving Problem 19, *all* observations $o(r, a, t)$, including the observations of previously-optimized spacecraft,

are considered in Equation (19b), ensuring that no point is observed twice. The coverage problem is submodular; therefore, if each spacecraft’s orbit is selected so as to maximize the reward of Problem (19), the greedy algorithm achieves an $(1 - 1/e)$ approximation of the optimum [31] for the overall set of spacecraft.

To select an (approximately) optimal orbit for an individual spacecraft, we simply sample a large number of candidate initial conditions, solve Problem (19) for each, and return the set of initial conditions that maximize the reward of (19a). The sampling approach is *not* guaranteed to be optimal, but it is a reasonable first-order approach for comparison purposes.

Sampling approach Both Algorithm 1 and the communication-agnostic optimizer critically rely on sampling of spacecraft orbits to initialize the gradient descent process. To this end, we sample the initial positions of instrument-carrying spacecraft with uniform probability within a cube centered on the small body, with each side equal to twice the diameter of the sphere enclosing the body. The magnitude and tangent plane of the initial velocity are selected to yield a circular orbit; the direction of the velocity vector in the tangent plane is selected uniformly at random, resulting in uniformly random inclination in $[-\pi/2, \pi/2]$ and uniformly random right ascension of the ascending node in $[-\pi, \pi]$.

Results Comparison are shown in Table 2 and Figure 7. Tables 3 and 4 report the orbital elements of the optimized orbits, and Figure 8 shows the bandwidth between spacecraft in the communication-aware and communication-agnostic cases.

	$B_0 = 10$ kbps		$B_0 = \infty$
	Comm-aware	Comm-agnostic	Comm-agnostic
Reward	595.9	354.9	1665.53
Number of regions observed	768	511	3270
by cameras	0	1	948
by imaging spectrometers	313	56	924
by X-Ray spectrometer	446	453	437
by altimeter	9	1	961
Avg. observability	0.324	0.329	0.334
by cameras	-	0.436	0.369
by imaging spectrometers	0.323	0.326	0.319
by X-Ray spectrometer	0.327	0.331	0.316
by altimeter	0.186	0.017	0.323

Table 2 Comparison of communication-aware and communication-agnostic orbit optimization.

The communication-aware approach results in a 67.9% higher reward compared to the greedy communication-agnostic approach, the result of a 50.3% increase in the number of regions observed and a focus on higher-value observations. Remarkably, the communication-aware approach is able to increase the number of high-value imaging spectrometer observations more than *fivefold* compared to the communication-agnostic approach, while also slightly

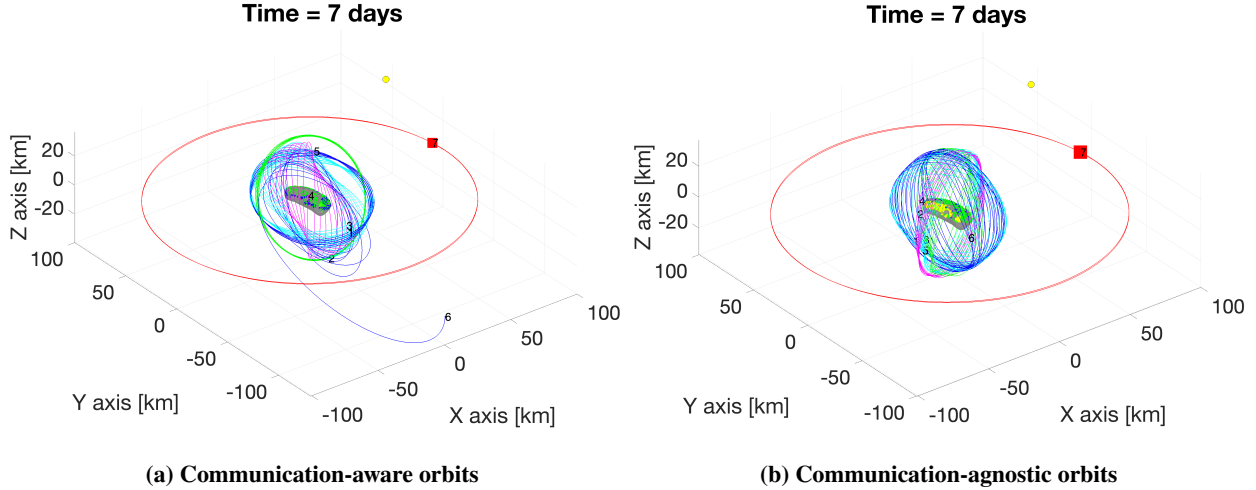


Fig. 7 Comparison of optimized orbits: communication-aware vs. communication-agnostic optimizer.

Table 3 Orbital elements of the optimized *communication-aware* orbits.

SC #	Instrument	a [m]	e	i [°]	Ω [°]	ω [°]	$\theta(0)$ [°]
1	Imaging Spectrometer	35324	0.000201	26.52	356.62	48.87	189.52
2	X Ray Spectrometer	35299	0.000705	117.99	178.46	153.38	176.84
3	Camera	35370	0.000791	25.92	8.15	234.63	355.60
4	Altimeter	35352	0.000368	148.80	232.18	93.97	359.71
5	Camera	35333	0.000030	161.22	235.82	250.85	178.97
6	Imaging Spectrometer	33405	0.039912	68.45	34.81	98.38	183.82
7	Carrier	100000	0.000000	0.00	0.00	0.00	0.00

increasing the number of X-Ray spectrometer and altimeter data points collected. Conversely, decoupling the problems of optimizing observations and optimizing communications results in remarkably poor performance: while the communication-agnostic orbits are able to *collect* large amounts of data, as shown in the rightmost column of Table 2, only a small fraction of the data can be relayed to the carrier due to the limited bandwidth between the spacecraft, resulting in most observations being lost.

Inspection of the orbital elements shown in Table 3 suggests that the optimization process exploits small changes in eccentricity and semi-major axis to achieve significantly higher bandwidth between key spacecraft pairs, resulting in more data throughput to the carrier with a minimal impact on observability. Figure 8 shows the overall bandwidth available between all spacecraft through the optimization horizon. The communication-aware orbits actually provide slightly *less* overall bandwidth between the spacecraft. However, more bandwidth is available between key spacecraft pairs: in particular, the communication-aware orbits provide significantly more bandwidth between one of the data-rich imaging spectrometers and the carrier, and they also offer a very large amount of bandwidth between the second spectrometer and a camera-carrying spacecraft which, in turn, acts as a relay to the carrier. In contrast, the altimeter

Table 4 Orbital elements of the optimized *communication-agnostics* orbits

SC #	Instrument	a [m]	e	i [°]	Ω [°]	ω [°]	$\theta(0)$ [°]
1	Imaging Spectrometer	35334	0	101.63	257.79	134.33	270.00
2	X Ray Spectrometer	35334	0	105.96	39.36	111.17	219.49
3	Camera	35334	0	84.74	264.96	49.45	355.08
4	Altimeter	35334	0	101.32	25.63	59.83	348.36
5	Camera	35334	0	105.17	30.13	224.52	90.00
6	Imaging Spectrometer	35334	0	96.19	118.90	147.65	270.00
7	Carrier	100000	0	0.00	0.00	0.00	0.00

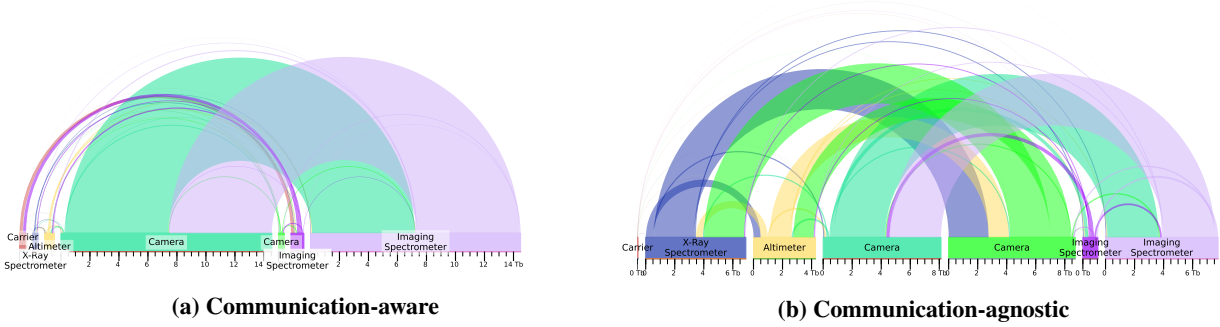


Fig. 8 Overall available bandwidth between the spacecraft throughout the optimization horizon. The x axis denotes the overall amount of bandwidth (in bits) available to be sent or received by each spacecraft. Arcs denote the amount of available bandwidth between spacecraft pairs; the color of each arc identifies the transmitter.

and the X-ray spectrometer, which generate much lower data volumes, see significantly less available bandwidth in the communication-aware case; however, due to the low data volume of these instruments, this only has a minor impact on the amount of science data collected. This perhaps counterintuitive results highlights the promise of the proposed approach: numerical optimization can identify targeted and highly granular opportunities for improvement in communications, resulting in a measurable increase in science returns.

We also assessed the performance of the proposed approach with a reference bandwidth of $B_0 = 250$ kbps at 100 km. In this communication-rich environment, the performance of the proposed approach was virtually indistinguishable from the performance of the communication-agnostic approach — an unsurprising result, since the usefulness of communication-aware optimization decreases as inter-spacecraft communication ceases to be the bottleneck to data collection.

We observe that one of the orbits computed by the communication-aware approach drifts far from the asteroid at the end of the optimization horizon in Figure 7a. As discussed in Section V, this is an expected side effect of the fixed-horizon optimizer, which has no consideration for the stability of orbits beyond the optimization horizon. The integration of differentiable constraints on the final state of the spacecraft in Algorithm 1 is a critical direction for future research.

Overall, these results show that the proposed approach is able to successfully perform communication-aware optimization of observation-gathering orbits around bodies with irregular gravity fields, outperforming communication-agnostic approaches and enabling the efficient design of multi-spacecraft missions to small solar system bodies.

Effectiveness of local optimization Finally, we turn our attention to assessing the effectiveness of the gradient-based trust region optimization step. The proposed algorithm interleaves sampling and local optimization, and it is natural to wonder whether the local optimization has a significant effect on the overall solution quality. To explore this, we compute the ratio between the reward obtained with the sampled initial conditions and the locally optimal reward produced by the trust region algorithm for fifty sets of initial conditions. Figure 9 shows the ratio between the reward at the initial sampled point and the locally optimal reward returned by the trust region algorithm.

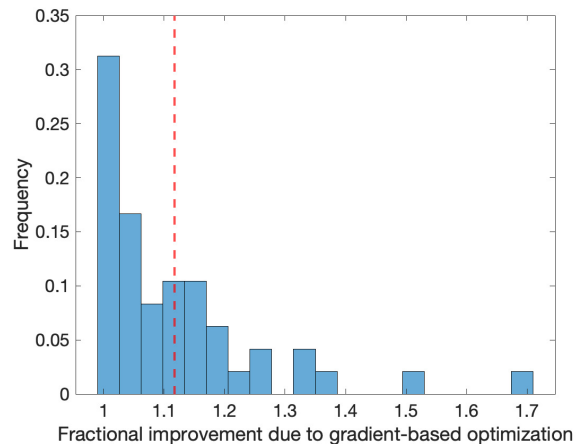


Fig. 9 Ratio between locally optimal reward and reward of initial sampled orbits.

The gradient-based optimization yields significant improvements compared to the initial guess, with an average 11.7% improvement in the solution quality due to local optimization. This suggests that gradient-based optimization, deployed as part of a global search strategy, can be an effective way of exploring the search space and identifying high-quality orbits for a multi-spacecraft mission around a small body, especially in bandwidth-constrained settings.

VII. Conclusions

Multi-spacecraft architectures hold promise to deliver increased science returns and shorter mission durations compared to monolithic mission architectures. Due to DSN capacity limitations and low available broadcast power, it is likely that such missions would require use of a dedicated “carrier” spacecraft to relay communications to and from Earth, and extensive inter-spacecraft communications to relay collected data from the instruments to the carrier. In this paper, we formulate the problem of communication-aware orbit optimization for such a spacecraft swarm, and we propose an efficient algorithm to solve the problem. Our simulation results demonstrate the feasibility of our proposed method, and

show that it can provide significant increased in science returns compared to communication-agnostic approaches in communication-constrained scenarios. An implementation of our algorithms is available under a permissive open-source license at <https://github.com/nasa/icc>.

A number of directions for future research are of interest. First, we plan to extend the proposed algorithmic formulation to capture long-term orbit stability constraints and ΔV budget constraints. Second, we plan to refine the proposed observability functions to capture other classes of instruments that introduce coupling between the spacecraft, e.g. radio science observations where a pair of spacecraft observes local transmissions to infer relative motion. Third, we plan to extend the problem formulation to capture data routing protocols other than Delay-Tolerant Networking, e.g. Ad-hoc On-Demand Distance Vector (AODV) routing[32]. And, finally, we plan to validate these results with a high-fidelity simulator that combines a popular orbital dynamic simulation software, GSFC's 42 [33], and a high-fidelity communication network simulator, ns-3 [34].

VIII. Acknowledgment

Part of this research was carried out at the Jet Propulsion Laboratory, California Institute of Technology, under a contract with the National Aeronautics and Space Administration (80NM0018D0004). ©2022. All rights reserved.

References

- [1] Rossi, F., Bandyopadhyay, S., Mote, M., de la Croix, J.-P., and Rahmani, A., "Communication-Aware Orbit Design for Small Spacecraft Swarms around Small Bodies," *AIAA/AAS Astrodynamics Specialist Conference*, 2020.
- [2] Glassmeier, K.-H., Boehnhardt, H., Koschny, D., Kührt, E., and Richter, I., "The Rosetta Mission: Flying Towards the Origin of the Solar System," *Space Science Reviews*, Vol. 128, No. 1-4, 2007, pp. 1–21. <https://doi.org/10.1007/s11214-006-9140-8>.
- [3] Fujiwara, A., Kawaguchi, J., Yeomans, D., Abe, M., Mukai, T., Okada, T., Saito, J., Yano, H., Yoshikawa, M., Scheeres, D., et al., "The rubble-pile asteroid Itokawa as observed by Hayabusa," *Science*, Vol. 312, No. 5778, 2006, pp. 1330–1334. <https://doi.org/10.1126/science.1125841>.
- [4] Tsuda, Y., Yoshikawa, M., Abe, M., Minamino, H., and Nakazawa, S., "System design of the Hayabusa 2 – Asteroid sample return mission to 1999 JU3," *Acta Astronautica*, Vol. 91, 2013, pp. 356–362.
- [5] Nolan, M. C., Magri, C., Howell, E. S., Benner, L. A., Giorgini, J. D., Hergenrother, C. W., Hudson, R. S., Lauretta, D. S., Margot, J.-L., Ostro, S. J., and Scheeres, D. J., "Shape model and surface properties of the OSIRIS-REx target Asteroid (101955) Bennu from radar and lightcurve observations," *Icarus*, Vol. 226, No. 1, 2013, pp. 629–640. <https://doi.org/10.1016/j.icarus.2013.05.028>.
- [6] Prockter, L., Murchie, S., Cheng, A., Krimigis, S., Farquhar, R., Santo, A., and Trombka, J., "The NEAR Shoemaker mission to asteroid 433 Eros," *Acta Astronautica*, Vol. 51, No. 1, 2002, pp. 491–500. [https://doi.org/10.1016/S0094-5765\(02\)00098-X](https://doi.org/10.1016/S0094-5765(02)00098-X).

- [7] Rayman, M. D., and Mase, R. A., “Dawn’s exploration of Vesta,” *Acta Astronautica*, Vol. 94, No. 1, 2014, pp. 159–167. <https://doi.org/https://doi.org/10.1016/j.actaastro.2013.08.003>, URL <https://www.sciencedirect.com/science/article/pii/S0094576513003123>.
- [8] Dennison, K., and D’Amico, S., “Comparing Optical Tracking Techniques in Distributed Asteroid Orbiter Missions Using Ray-Tracing,” *AAS/AIAA Space Flight Mechanics Meeting*, 2021. Paper AAS 21-336.
- [9] Stacey, N., and D’Amico, S., “Autonomous swarming for simultaneous navigation and asteroid characterization,” *AAS/AIAA Astrodynamics Specialist Conference*, 2018.
- [10] Stacey, N., Dennison, K., and D’Amico, S., “Autonomous Asteroid Characterization through Nanosatellite Swarming,” *IEEE Aerospace Conference*, IEEE, 2022, pp. 1–21.
- [11] Mortari, D., Wilkins, M. P., and Bruccoleri, C., “The flower constellations,” *Journal of Astronautical Sciences*, Vol. 52, No. 1, 2004, pp. 107–127. <https://doi.org/10.1007/BF03546424>.
- [12] Mortari, D., and Wilkins, M. P., “Flower constellation set theory. Part I: Compatibility and phasing,” *IEEE Transactions on Aerospace and Electronic Systems*, Vol. 44, No. 3, 2008, pp. 953–962. <https://doi.org/10.1109/TAES.2008.4655355>.
- [13] Nag, S., Li, A. S., and Merrick, J. H., “Scheduling algorithms for rapid imaging using agile Cubesat constellations,” *Advances in Space Research*, Vol. 61, No. 3, 2018, pp. 891–913. <https://doi.org/10.1016/j.asr.2017.11.010>.
- [14] Hernandez, S., Stuart, J. R., Garza, D. M., Broschart, S. B., Herzig, S. J., and Chien, S. A., “Satellite Constellation Orbit Design to Enable a Space-Based Radio Interferometer,” *AAS/AIAA Astrodynamics Specialist Conference*, 2017.
- [15] Stuart, J., Dorsey, A., Alibay, F., and Filipe, N., “Formation flying and position determination for a space-based interferometer in GEO graveyard orbit,” *IEEE Aerospace Conference*, IEEE, 2017, pp. 1–19.
- [16] Villa, J., French, A., McMahon, J., Scheeres, D., and Hockman, B., “Gravity estimation at small bodies via optical tracking of hopping artificial probes,” *AIAA/AAS Astrodynamics Specialist Conference*, 2021.
- [17] Koenig, A. W., and D’Amico, S., “Robust and safe N-spacecraft swarming in perturbed near-circular orbits,” *Journal of Guidance, Control, and Dynamics*, Vol. 41, No. 8, 2018, pp. 1643–1662. <https://doi.org/10.2514/1.G003249>.
- [18] Lippe, C., and D’Amico, S., “Spacecraft swarm dynamics and control about asteroids,” *Advances in Space Research*, Vol. 67, No. 11, 2021, pp. 3426–3443. <https://doi.org/10.1016/j.asr.2020.06.037>.
- [19] Hernandez, S., Bandyopadhyay, S., Haynes, M., Karimi, R., and Anderson, R., “Two-spacecraft orbiting in opposition to enable bistatic radar observations around an asteroid,” *AIAA/AAS Astrodynamics Specialist Conference*, 2021.
- [20] Burleigh, S., Hooke, A., Torgerson, L., Fall, K., Cerf, V., Durst, B., Scott, K., and Weiss, H., “Delay-tolerant networking: an approach to interplanetary Internet,” *IEEE Communications Magazine*, Vol. 41, No. 6, 2003, pp. 128–136. <https://doi.org/10.1109/MCOM.2003.1204759>.

- [21] Broschart, S. B., Abrahamson, M., Bhaskaran, S., Fahnestock, E. G., Karimi, R., Lantoine, G., Pavlak, T. A., and Chappaz, L., “The small-body dynamics toolkit and associated close-proximity navigation analysis tools at JPL,” *AAS Guidance and Control Conference*, 2015, pp. 1–12.
- [22] van Nee, R., Awater, G., Morikura, M., Takanashi, H., Webster, M., and Halford, K., “New high-rate wireless LAN standards,” *IEEE Communications Magazine*, Vol. 37, No. 12, 1999, pp. 82–88. <https://doi.org/10.1109/35.809389>.
- [23] “IEEE Standard for Information technology– Local and metropolitan area networks– Specific requirements– Part 11: Wireless LAN Medium Access Control (MAC) and Physical Layer (PHY) Specifications Amendment 5: Enhancements for Higher Throughput,” *IEEE Std 802.11n-2009 (Amendment to IEEE Std 802.11-2007 as amended by IEEE Std 802.11k-2008, IEEE Std 802.11r-2008, IEEE Std 802.11y-2008, and IEEE Std 802.11w-2009)*, 2009, pp. 1–565.
- [24] Ahuja, R. K., Magnanti, T. L., and Orlin, J. B., *Network Flows: Theory, Algorithms and Applications*, Prentice Hall, 1993.
- [25] Scheeres, D. J., *Orbital motion in strongly perturbed environments: applications to asteroid, comet and planetary satellite orbiters*, Springer, 2016.
- [26] Byrd, R. H., Hribar, M. E., and Nocedal, J., “An interior point algorithm for large-scale nonlinear programming,” *SIAM Journal on Optimization*, Vol. 9, No. 4, 1999, pp. 877–900. <https://doi.org/10.1137/S1052623497325107>.
- [27] Byrd, R. H., Gilbert, J. C., and Nocedal, J., “A trust region method based on interior point techniques for nonlinear programming,” *Mathematical programming*, Vol. 89, No. 1, 2000, pp. 149–185.
- [28] Gill, P. E., Murray, W., and Wright, M. H., *Practical Optimization*, Society for Industrial and Applied Mathematics, Philadelphia, PA, 2019. <https://doi.org/10.1137/1.9781611975604>.
- [29] Zilberstein, S., “Using Anytime Algorithms in Intelligent Systems,” *AI Magazine*, Vol. 17, No. 3, 1996, p. 73. <https://doi.org/10.1609/aimag.v17i3.1232>, URL <https://ojs.aaai.org/index.php/aimagazine/article/view/1232>.
- [30] Kobayashi, M. M., “State-of-the-Art Status for Deep-Space SmallSat Telecom,” 2018 International Planetary Probe Workshop Short Course on Small Satellites, Jun. 2018. URL <http://hdl.handle.net/2014/49860>.
- [31] Nemhauser, G. L., Wolsey, L. A., and Fisher, M. L., “An analysis of approximations for maximizing submodular set functions—I,” *Mathematical programming*, Vol. 14, No. 1, 1978, pp. 265–294. <https://doi.org/10.1007/BF01588971>.
- [32] Perkins, C., Belding-Royer, E., and Das, S., “RFC3561: Ad hoc on-demand distance vector (AODV) routing,” 2003.
- [33] Stoneking, E., “42: An Open-Source Simulation Tool for Study and Design of Spacecraft Attitude Control Systems,” <https://github.com/ericstoneking/42>, 2020.
- [34] Riley, G. F., and Henderson, T. R., “The ns-3 Network Simulator,” *Modeling and Tools for Network Simulation*, edited by K. Wehrle, M. Güneş, and J. Gross, Springer Berlin Heidelberg, Berlin, Heidelberg, 2010, pp. 15–34. https://doi.org/10.1007/978-3-642-12331-3_2.